Noname manuscript No.
(will be inserted by the editor)

Partially Camouflaged Object Tracking using Modified Probabilistic Neural Network and Fuzzy Energy based Active Contour

Ajoy Mondal · Susmita Ghosh · Ashish Ghosh

the date of receipt and acceptance should be inserted later

Abstract Various problems in object detection and tracking have attracted researchers to develop methodologies for solving these problems. Occurrence of camouflage is one of such challenges that makes object detection and tracking problems more complex. However, less attention has been given to detect and track camouflaged objects due to complexity of the problem. In this article, we propose a tracking-by-detection algorithm to detect and track camouflaged objects. To increase separability between the camouflaged object and the background, we propose to integrate features (CIELab, histogram of orientation gradients and locally adaptive ternary pattern) from multi-cue (color, shape and texture) to represent a camouflaged object. A probabilistic neural network (PNN) is modified to construct an efficient discriminative appearance model for detecting camouflaged objects in video sequences. A large number of training patterns (many could be redundant) are reduced based on motion of the object in the modified PNN. The modified PNN makes the detection process faster and also increases the detection accuracy. Due to high visual similarity among the camouflaged object and the background, the boundary of camouflaged object is not well defined (i.e., boundary may be smooth and/or discontinuous). In this context, a robust fuzzy energy based active contour model using both global and local information is proposed to extract contour (boundary) of the detected camouflaged object for tracking. We show a realization of the proposed method and demonstrate its performance (both quantitatively and qualitatively) with respect to state-of-the-art techniques on several challenging sequences. Analysis of results concludes that the proposed technique can track camouflaged (fully or partially) objects as well as objects in various complex environments in a better way as compare to the existing ones.

Keywords Camouflage, multi-cue, probabilistic neural network, fuzzy energy and visual similarity.

A. Mondal · A. Ghosh
Machine Intelligence Unit, Indian Statistical Institute, Kolkata-700108, India
email: ajoy.mondal83@gmail.com
A. Ghosh
email: ash@isical.ac.in
S. Ghosh
Department of Computer Science and Engineering, Jadavpur University, Kolkata, 700032, India
email: susmitaghoshju@gmail.com

1 Introduction

Moving object[1] tracking from a given video sequence has a great deal of interest in computer vision and has been an active research area for the last few decades [46, 76, 79, 82]. It can be defined as the problem of estimating the trajectory of an object of interest in a video sequence. It is widely used in automated surveillance system [47, 79], traffic monitoring [79], vehicle navigation [79], activity recognition and anomaly detection [46], medical application and biological research [4, 47], etc. It is a challenging task because of camouflaged objects, presence of noise in the image frames, complex object motion, partial or full object occlusion, background clutter, illumination variation, complex object shapes, large variation in object scale and orientation, etc [18,46,69,79,82]. In literature, various tracking techniques [2, 3, 26, 29, 32, 34, 40, 59–61, 76, 77, 81, 82, 84] are developed to handle such problems and there exists no single algorithm which can successfully handle all these factors.

[1] In this article, the words object and target are used interchangeably

1.1 Review on Visual Tracking

Recently, visual object tracking has been posed as a tracking-by-detection problem [2], where statistical modeling is dynamically performed for detecting an object. Various statistical (generative and discriminative) appearance modelings are very popular in the literature to track an object. The main focus of generative appearance model is to accurately fit the data from the object class. In practice, it is very difficult to verify the correctness of the specified model [46]. It also provides local optimal solutions due to the (sub optimal) parameters. Optimal results may be obtained by introducing online updating mechanism. However, during updating, it incrementally learns only the representation of foreground object ignoring the influence of the background. As a result, they often suffer from the distractions caused by the background regions with similar appearance to the object class [46]. On the other hand, discriminative appearance models pose object tracking as a binary classification problem. Its aim is to find out a decision boundary which maximizes the separability between the object and its surroundings. To cope with changes in the object appearance as well as the background (due to both the object and the camera motions), the tracker needs to be adaptive. Thus, they can achieve effective and efficient performances [46].

In literature, several techniques [2, 3, 26, 29, 32, 34, 40, 59, 61, 76, 77, 81, 82, 84] have been developed based on discriminative, generative and combination of both discriminative & generative appearance models. Among them, VTD [40], ASLA [32], MTT [81] and SCM [84] are based on generative appearance model. Sparse representations are used in all these techniques. These representations are effective to account for appearance changes (e.g., partial occlusion, pose changes, etc). All these methods provide good results for video sequences having such complexities. However, local sparse representation (used in VTD [40], ASLA [32] and SCM [84]) is more effective than global sparse representation (used in MTT [81]). Particle filter is used to locate the object in the next frame in all these methods. Incase of fast moving object, these methods produce unsatisfactory results.

On the other hand, several algorithms [2,3,26,34,40, 60, 61, 81] based on discriminative appearance models have been developed for visual tracking. In all these approaches, the discriminative appearance models are considered as base classifiers to distinguish the object from its surrounding.

The ensemble tracker [2] poses tracking as a pixel based binary classification problem. Changes in the object appearance can be handled by adding new weak classifiers to the ensemble system. Although this method is able to distinguish the object from its background, it is unable to handle the changes in pose, scale and orientation of the object, full & long time occlusion and background clutter. To reduce the drift problem, Babenko *et al.* [3] proposed an online multiple instance learning for object tracking. This technique can take care of partial occlusion, scale change; but is unable to cope with full or long time occlusion, large variation in scale and orientation.

In these tracking-by-detection techniques, appearance models are adaptive to take into account changes caused by object motion, illumination variation and occlusion. From the estimated object location, a set of binary labeled training samples is generated to update the classifier online. However, the generated training set is not always correct (with respect to the object and the background classes), and reduces tracking accuracy. To solve this problem, Hare *et al.* proposed structure output tracking with kernels (Struck) [26] which integrates learning and tracking, avoiding the need for ad-hoc update strategies. In [34], Kalal *et al.* proposed a novel tracking algorithm with appearance learning approach which combines nearest neighbor (NN) classifier with median of particle optical flow tracker. It is able to deal with appearance change, illumination variation, pose change, scale variation and background clutter.

Most of the trackers use high-level appearance structures or low-level cues for detecting and tracking objects. In [77], Yang *et al.* proposed a discriminative appearance model based on superpixels, to distinguish the target and the background with mid-level cues. Target location in the next frame is estimated by maximizing a posterior probability based on the object background confidence map. It can handle heavy occlusion and recover the tracker from drift problem. Though all the discussed methods are able to track object in several complex environments, they are computationally more expensive. In [29], Henriques *et al.* proposed kernelized correlation filter (KCF) based on fast Fourier transforms to distingue object from its surroundings. It is faster than all other existing tracking algorithms with better performance.

From the above discussion, it is highlighted that the behaviors of all these techniques are not explicitly mentioned to track camouflaged objects. Occurrence of camouflage makes object tracking more complex [14, 63].

1.2 Review on Feature based Robust Visual Representation of Target (Object)

Visual representation reflects the statistical characteristics of object appearance [46,47]. It plays an important role in object detection and tracking scenario. Various features are proposed or considered to represent objects for detection and tracking [9, 47]. Features generated from single-cue (like color or shape or texture or motion) is considered in detection and tracking techniques [9, 46, 47]. On the other hand, features generated from multi-cue (like color, shape, texture and motion) have also been widely used in detection and tracking system [41, 54, 72]. It is observed that multi-cue is better than single-cue in the context of object detection and tracking [41, 54, 72]. In [72], color and shape features are integrated to track objects in mean shift framework. The authors considered color histogram in three color spaces RGB, HSV, normalized rg and histogram of gradient orientation to describe shape. This method is time consuming and is unable to track objects under several conditions like illumination variation, similar background objects (clutter) and camouflaged object. To track objects in cluttered background, Ning *et al.* [54] integrated histograms of color and texture in mean shift framework. It provides better results than the mean shift tracking using only color histogram. However, this method is not robust for several conditions like illumination variation, pose variation and camouflaged objects; and is also time consuming. In [41], particle filter based multi-cue (e.g. color and shape) tracking framework is proposed to increase the tracking performance in several complex environments like illumination variation, occlusion and pose variation. Basically, in all these methods, histograms generated from multi-cue are integrated for tracking objects.

1.3 Review on Camouflaged Object Detection and Tracking

Camouflage is an attempt to conceal the signature of a target into the background [14, 23]. In other words, camouflage is the ability of prey to hide themselves from predators by changing their body patterns, texture and coloration as per environment's texture. Work related to camouflage can be roughly divided into two major areas: (i) camouflage assessment and design, (ii) camouflage detection [14,23,63]. Camouflage design system artificially creates camouflage images [19]; whereas, camouflage detection is used to extract the target from the background. It basically discriminates the camouflaged foreground object from background [14, 23, 63]. Camouflage detection systems have many potential applications including (i) preserving wildlife, (ii) target detection in the battle field, (iii) defect detection during manufacturing, (iv) identification of duplicate products during logistics, etc.

In literature, various techniques [6, 11, 13, 27, 30, 31, 33, 48] are developed to detect camouflaged objects. Harville *et al.* [27] proposed a foreground segmentation technique using both color and depth information to detect camouflaged objects. Information loss occurs due to the projection of 3D scene into 2D picture. Here, depth information is considered to reduce the information loss for 3D to 2D projection. Use of depth information increases the detection accuracy and also increases the computational cost. In this direction, Boult *et al.* [6] developed a camouflaged object detection technique using background subtraction with consideration of two thresholds. Here, larger threshold is considered to detect pixels which are certainly in the foreground. Whereas, smaller threshold is used to detect uncertain pixels (i.e., pixels which are part of either background or camouflaged object). Then quasi connected component is taken into consideration to detect camouflaged target. The detection accuracy is highly dependent on threshold values. Selection of proper threshold value itself is a problem. For slow moving objects, this method fails to detect objects. In [33], Pong and Bowden proposed a technique with the help of stochastic process to handle camouflage. This algorithm assumes that camouflage occurs when the new observation can not be associated with an existing task. Basically, performance of this method depends on color and motion of the object. Here, color is used to distinguish the camouflaged object and its surrounding whereas motion is considered to separate out moving objects and static parts of the frame. Hence, both these information help to detect moving camouflaged object. Sometimes, this method may fail for an object which is very much similar to its background and background contains more non-static objects.

Hung and Jiang [31] devised a method to track camouflaged objects using sequential execution of two techniques. An iterative region consolidation operator is used to fill the gaps introduced by camouflage. Then active contour model is built during tracking to capture the actual shape of the target. Basically, performance of this method relies on the inter-frame difference. If the object has slow motion, it is very difficult to localize the object using iterative weighted region consolidation operator. Hence, tracking may fail for sequences containing slow moving and uniform colored objects. To detect camouflaged object, Chandesa *et al.* [11] proposed an algorithm based on particle filter, in

which Gaussian mixture model of particle distribution is considered to investigate the effect of camouflage on the particle set representing the object. This method works well on occluded object but not for camouflaged object. Though this method works well it needs object information (a priori) to execute the algorithm. In [13], Conte *et al.* proposed an algorithm to detect partially camouflaged people. They have used background subtraction technique to detect different parts of people. Then grouping of different parts is performed based on the shape of targets. This method is unable to provide satisfactory results for objects other than human. Also it is not always possible to extract the actual shape of the object by combining different detected parts of the object.

In this direction, Yin *et al.* [30] developed an algorithm to track mobile camouflaged objects based on optical flow model. Optical flow model is used to detect motion patterns corresponding to the camouflaged object and the background. Based on magnitude and location of the optical flow, motion patterns are clustered to detect the camouflaged object. Thereafter, Kalman filter is considered to improve the detection accuracy. However, the accuracy of this technique highly depends on the result of optical flow. For slow moving objects and objects with camera motion, this method fails to provide good results. Recently, Malathi and Bhuyan [48] developed a background subtraction scheme using multi-view information to detect camouflaged object. Here, pixels corresponding to the background are quantized into codebooks which are sufficient to represent a background. Codebooks extracted from each frame corresponding to each camera are combined to construct a background and the objects are detected by subtracting constructed background from the frame. This method provided good results for occluded objects however, unable to provide satisfactory results for camouflaged objects.

1.4 Review on Fuzzy Active Contour

Kass *et al.* [35] introduced the active contour (snake) model (ACM) to detect and track objects. The main idea behind the ACM is based on deformation of an initial curve so that it evolves towards the object boundary under some constraints. It has the ability to generate closed parametric curve [15]. However, it has some drawbacks such as: (i) segmentation results highly depend on initial contour position, (ii) it is easily deteriorated by noise present in the given image. Several approaches [8, 12, 45, 78] based on ACMs have been developed to overcome such drawbacks to some extend.

Active contour and its variants are basically "edge based" models which use image gradient to attract the contour towards the object boundaries. As these models rely on edge information, sometimes it may fail to extract contour when the gradient of the object boundaries is not well defined for noisy, blurred or even discontinuous edged images.

Different from "edge based" active contours, "region based" active contour models [10, 37, 42, 70, 74, 80] using region information like intensity, color and texture features are also introduced in the literature.

In general, the "region based" models use image information from not only the evolving contours but also from the image statistics inside and outside the contour. Chen and Vese [10] proposed an active contour (Chen-Vese) model which depends on the region based energy function, inspired by Mumford-Shush function [52]. In this model, two regions inside and outside the contour in the image are assumed to be homogeneous. Here, the global image (statistics) information is used in the energy function to transform it into the level set formulation. The Chen-Vese model as well as other region based models are able to deal with images having weak boundaries. In addition, they are less sensitive to the initial contour position as compared to the "edge based" model.

Some modifications in the Chen-Vese model have been proposed in the literature [37, 42, 67, 80] mainly to reduce the high computational cost. In [37], Krinidis and Chatzis proposed a "region based" active contour model to segment images. This model uses global image information which is able to segment images with blur and discontinuous boundaries and is robust to the initial position of the contour. In this model, they assumed that the image is approximated with two regions of piece-wise constant intensities inside and outside the contour. However, this model is unable to produce good segmentation for images containing intensity inhomogeneity or non-homogeneity.

In fact, real life images contain intensity inhomogeneity or non-homogeneity which makes the segmentation a more challenging problem. To segment such kinds of images, region based active contours using local image (statistics) information are proposed in the literature [42, 80]. However, all these models are unable to produce good results for highly blurred, noisy and intensity inhomogeneity images.

To overcome such drawbacks, "region based" active contours using both global and local information are developed in the literature [38, 62]. In both these methods, local information, based on only the spatial distance is considered and they are not robust to high level of blur,

noise and intensity inhomogeneity or non-homogeneity present in the images.

1.5 Contribution and Basic Workflow of the Proposed Algorithm

In this article, a tracking-by-detection algorithm is proposed to detect and track camouflaged objects in video scenes. The proposed work has three main contributions:

i: Integration of (CIELab, histogram of orientation gradients and locally adaptive ternary pattern) features from multi-cue (color, shape and texture) to increase separability between the camouflaged object and the background.
ii: A discriminative appearance model is proposed by modifying a probabilistic neural network to detect camouflaged objects.
iii: A fuzzy energy based active contour model using both the global and local information is proposed to track camouflaged objects.

When visual characteristics (like color or texture or shape or all of them) of the objects are too similar to the background, camouflage occurs [63]. The objective of a camouflage detection system is to separate the camouflaged object from background. In such cases, features generated from single-cue (like color or texture or shape or motion) is not sufficient to extract camouflaged objects from background because the underlying phenomenon for occurrence of camouflage is not known. In this context, integration of features generated from multi-cue (color, texture, shape, motion, etc.) may increase the separability between the camouflaged objects and background. As our goal is to detect and track the camouflaged objects, (CIELab, histogram of orientation gradients and locally adaptive ternary pattern) features from multi-cue (color, shape and texture) are integrated here to increase the separability between the camouflaged objects and the background.

The probabilistic neural network (PNN) [65] developed by Specht has became an efficient tool for solving many pattern classification and computer vision problems [24, 53, 75] due to its easy, non iterative training process and statistical foundation in Bayesian estimation theory. It has the ability to produce good classification results in complex classification problems. Recently, object tracking is posed as a binary classification (single object) problem [2]. Occurrence of camouflage makes object detection and tracking problems more complex. In such complex scenario, to detect an object, PNN may be considered.

A discriminative appearance model is proposed by modifying a probabilistic neural network to detect camouflaged object in the target candidate frame. In PNN, the pattern layer contains all training patterns which may be redundant and it increases the network structure. This large network structure introduces two problems, (i) high computational cost is incurred to classify an unknown pattern because the amount of computation necessary to classify an unknown pattern is proportional to the size of the network [49, 71], (ii) due to the large network architecture, classifier is highly biased to the training patterns and exhibit poor generalization capacities to unseen data (i.e. overfitting problem) [5, 49, 71]. To solve these problems of PNN, one algorithm based on motion of the object is proposed to select training patterns (subset of training patterns). The proposed training pattern selection technique makes the classification process faster due to the reduced network architecture and increases the classification accuracy due to the consideration of training subset with local information instead of global information. Therefore, the proposed PNN provides better detection of the camouflaged objects.

Since camouflaged object is visually very similar to the background, boundary of the camouflaged object is not well defined (i.e., the boundary may be smooth and /or discontinuous). Due to motion of the object and the camera, boundary of the object in the frames extracted from a video sequence is blurred. However, the object regions in real life video sequence usually contain high intensity/color inhomogeneity or non-homogeneity. To extract boundary of such kinds of objects in images, fuzzy active contour models are proposed in literature [37, 74]. All these models use only global information and are unable to extract contours in such environment due to high visual similarity between the camouflaged object and the background. In this article, a robust fuzzy energy based active contour model using both global and local information is proposed to extract the contour (boundary) of the detected camouflage object for tracking. The contour is evolved iteratively with object detection results produced by the modified PNN as an initialization for the proposed fuzzy active contour model. Finally, camouflaged object is tracked by its contour.

To test the effectiveness of the proposed algorithm, investigation was carried out on 200 challenging video sequences containing (full or partial) camouflaged object, illumination variation, scale change, rotation, shape deformation, background clutter, pose change, partial or full occlusion, etc. Tracking results of the proposed method are compared with six state-of-the-art tracking algorithms. Evaluation measures such as average center

location error, average tracking accuracy (area overlap), precision plot and success plot are considered to evaluate the performance of the proposed technique. From the analysis (both quantitative and qualitative) of results, it is found that the proposed method performs favorably against state-of-the-art techniques on several sequences having different complexities.

Rest of the article is organized as follows. Section 2 describes the proposed technique for camouflaged object tracking. Experimental results and analysis are presented in Section 3. Discussion and future work are described in Section 4. Conclusive remarks are put in Section 5.

2 Proposed Technique for Partially Camouflaged Object Tracking

In this article, a tracking-by-detection algorithm has been developed to detect and track camouflaged objects. Color (CIELab), shape (histogram of orientation gradients) and textural (locally adaptive ternary pattern) features are integrated to represent the camouflaged object in the target frame. A discriminative appearance model is proposed by modifying a PNN to detect camouflaged objects in the target candidate frame. Finally, camouflaged objects are tracked in the target candidate frame by the proposed fuzzy energy based active contour model. Fig. 1 displays flowchart of the proposed tracking algorithm. Each part of the proposed tracking algorithm is described in the following subsections.

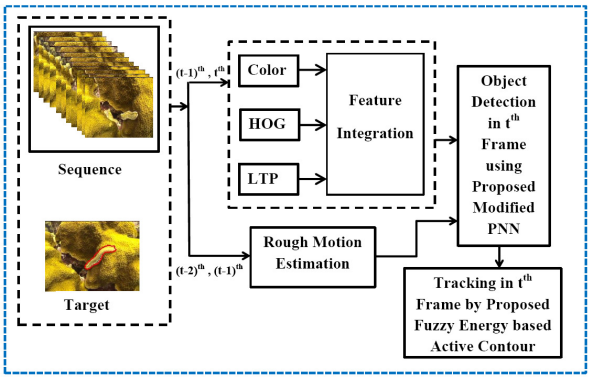

Fig. 1 Flowchart of the proposed tracking algorithm.

2.1 Multi-cue Feature based Robust Visual Representation

Camouflage occurs due to high visual similarity (with respect to color or texture or shape or all of them) among an object and its surroundings [63]. The objective of a camouflaged object detection technique is to extract the camouflaged object from the background. In this context, robust features are needed to detect the camouflaged object from its surroundings. As the objective of the present article is to detect and track camouflaged objects, robust features are needed to increase the separability between the camouflaged object and the background. In this article, color (CIELab), shape (histogram of orientation gradients) and textural features (locally adaptive ternary pattern) are integrated to increase the separability between the camouflaged object and the background.

2.1.1 Color Feature

In this article, color of the object is represented by CIELab color space. It is perceptually uniformed and is better to separate lightness from color compared to other color spaces [19]. It also indicates proper changes in the direction of human color perception. Its components are lightness of the color (L^*) and two color-opponent dimensions (a^* and b^*). The nonlinearity among L^*, a^* and b^* are intended to mimic the nonlinear response of the human eye [19]. Furthermore, uniform changes of components in the $L^*a^*b^*$ color space aim to correspond to uniform changes in the perceived color.

2.1.2 Shape Feature based on Histogram of Orientation Gradients

It has been widely used as a key feature for hand gesture recognition [21], face recognition [43], human detection [16], pedestrian detection [66] and object tracking [2]. It captures the local object appearance, shape and is invariant to local geometric and photometric transformations: translation or rotation [16]. It is also largely invariant to global illumination changes [43]. A shape is described by an orientation histogram which is computed based on image derivatives in x and y directions. The gradients at the point $\mathbf{X}$ in the image frame I can be calculated by convolving the Sobel mask [22] with the image. The gradients are defined as: $I_x(\mathbf{X}) = D_x * I(\mathbf{X})$ and $I_y(\mathbf{X}) = D_y * I(\mathbf{X})$, where D_x and D_y are Sobel masks in x and y directions, respectively. The magnitude of the gradient at the point $\mathbf{X}$ is computed as $G(\mathbf{X}) = \sqrt{I_x^2(\mathbf{X}) + I_y^2(\mathbf{X})}$. The orientation of gradient of that pixel is given by $\theta(\mathbf{X}) = \arctan\left(\frac{I_y(\mathbf{X})}{I_x(\mathbf{X})}\right)$. The orientations are quantized into 8 bins. Each orientation is weighted and assigned to one of the two adjacent bins according to its distance from the bin centers. For more details one can go through [16].

2.1.3 Locally Adaptive Texture Feature

Various statistical descriptors have been proposed to measure image texture in literature [25, 55, 68]. Among them, local ternary pattern (LTP) [68] is quite popular to solve various computer vision problems. As visual appearance of the camouflaged target is very similar to the background, local adaptive ternary pattern (LATP) [1] is considered to describe image texture in this article. LTP is an extension of local binary pattern (LBP) [55]. Here, instead of central pixel value of a neighborhood (small image region), thresholding is done based on user defined value Th. Any pixel value within a neighborhood laying within the interval of $[-Th,\ Th]$ of the central pixel is assigned a value 0. The pixel values above Th when compared to the central pixel are assigned to 1 and ones below $-Th$ when compared to the central pixel are assigned to -1. Thus, LTP of a pixel X is computed as

$$LTP(X) = \begin{cases} 1 & if \quad I(Y) - I(X) \geq Th \\ 0 & if \ -Th \leq I(Y) - I(X) \leq Th, \\ -1 & if \quad I(Y) - I(X) \leq -Th \end{cases} \quad (1)$$

where Th is a user defined threshold value, $I(\mathbf{X})$ and $I(\mathbf{Y})$ are intensity values of the central pixel and neighborhood pixels, respectively. LTP codes are more resistant to noise, but no longer strictly invariant to gray-level transformations. The LTP encoding procedure is illustrated in Fig. 2. Here the threshold Th was set to 5, so the tolerance interval is $[95, 105]$. Each ternary pattern is split into its positive and negative halves as illustrated in Fig. 3; these are called upper and lower patterns, respectively. However, performance of LTP depends on threshold value. Akhloufi and Bendada [1] proposed a locally adaptive ternary pattern (LATP) for multi-spectral face recognition. LATP code is extracted as

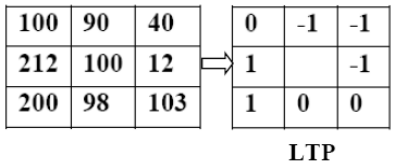

Fig. 2 Illustration of the basic LTP operator.

$$LATP(\mathbf{X}) = \begin{cases} 1 & if \ \ I(\mathbf{Y}) \geq (\mu_\eta + k\sigma_\eta) \\ 0 & if \ |I(\mathbf{Y})| < (\mu_\eta + k\sigma_\eta) \\ -1 & if \ I(\mathbf{Y}) \leq (\mu_\eta - k\sigma_\eta), \end{cases} \quad (2)$$

where μ_η and σ_η refer to the mean and standard deviation of pixel values in the neighborhood and k is a user defined constant.

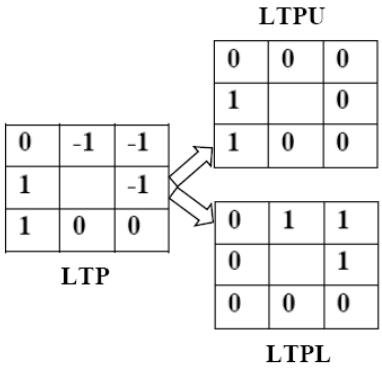

Fig. 3 Splitting a LTP code into positive (LTPU) and negative (LTPL) codes.

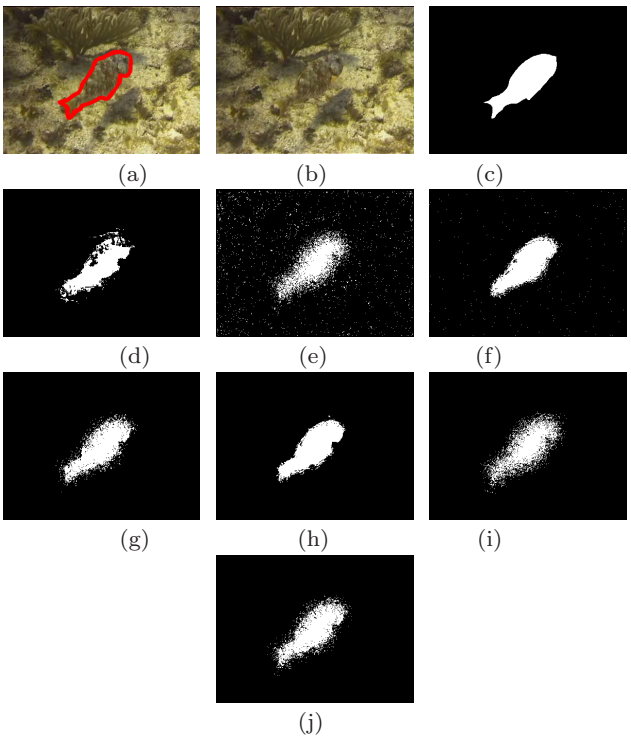

Fig. 4 Clip152 sequence (a) target frame; (b) target candidate frame; (c) ground truth. Object detection using the proposed modifying PNN ($\sigma = 0.1$) with consideration of (d) color feature; (e) shape feature; (f) texture feature; integration of (g) color and shape features; (h) color and texture features; (i) shape and texture features and (j) color, shape and texture features.

In this article, the normalized color (CIELab), shape (HOG) and texture (LTPU and LTPL) features are integrated to generate d-dimensional feature vectors. Then each frame is transformed into d-dimensional features space. Now each pixel $\mathbf{X}^t$ of the t^{th} frame is considered as a pattern $I(\mathbf{x}^t) \in \Re^d$ and is represented by $I(\mathbf{x}^t) = \left(f_{x_1^t}, f_{x_2^t}, .., f_{x_i^t}, .., f_{x_d^t}\right)$.

Figs. 4-6 highlight the object detection results in the target candidate frame using the proposed PNN (dis-

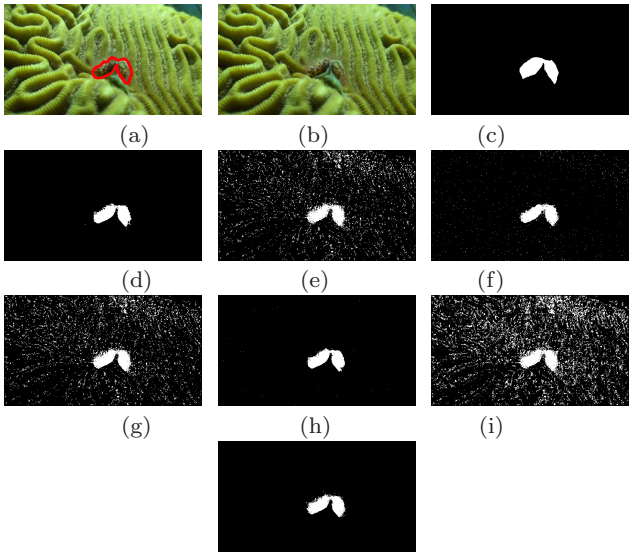

Fig. 5 Clip730 sequence (a) target frame; (b) target candidate frame; (c) ground truth. Object detection using the proposed modifying PNN ($\sigma = 0.1$) with consideration of (d) color feature; (e) shape feature; (f) texture feature; integration of (g) color and shape features; (h) color and texture features; (i) shape and texture features and (j) color, shape and texture features.

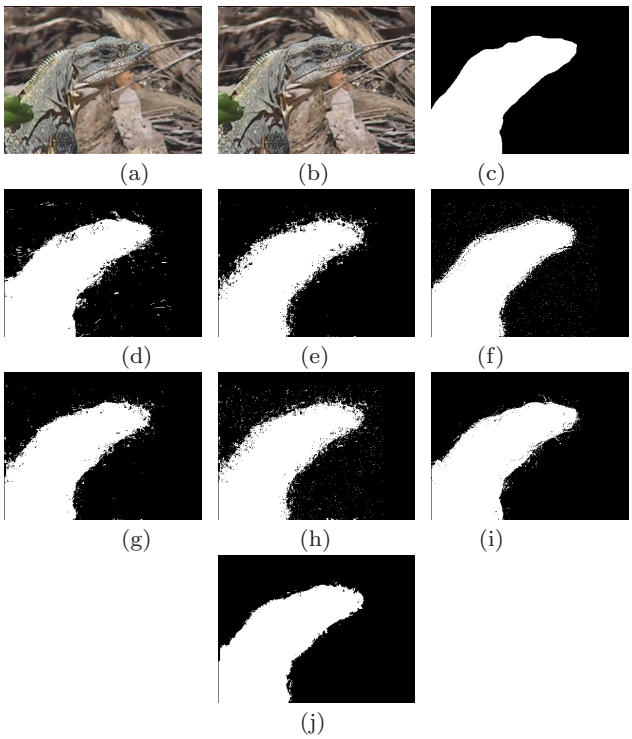

Fig. 6 Clip187 sequence (a) target frame; (b) target candidate frame; (c) ground truth. Object detection using the proposed modifying PNN ($\sigma = 0.1$) with consideration of (d) color feature; (e) shape feature; (f) texture feature; integration of (g) color and shape features; (h) color and texture features; (i) shape and texture features and (j) color, shape and texture features.

cussed in the next section) with smoothness parameter $\sigma = 0.1$ for all cases with different features and their various combinations for three video sequences. From Fig. 4, it is observed that texture feature individually is better than color and shape features for detecting camouflaged object in Clip152 sequence. In case of combination of two features, color & texture provide better results. However, combination of all features color, shape and texture provides best results among individual features and their other combinations for Clip152 sequence. On the other hand, for Clip730 sequence, color feature (individually) produces better detection result than shape and texture features. In case of combination of features, color & texture produce better results than other combinations of two features (i.e., color & shape and texture & shape). However, combination of color, shape and texture provides best results among individual features and their other combinations. In case of Clip187 sequence, shape feature is individually better than color and texture features. Among combinations of two features, texture & shape provide better results. However, combination of color, shape and texture provides the best result. From these figures, it is also observed that some features and their combinations produce better detection results for some sequences and for other sequences, these are unable to provide good results. On the other hand, integration of color, shape and texture features provides better object detection results than individual features and their other combinations for the camouflaged sequences. These examples highlight the superiority of integration of features from multi-cue for detecting camouflaged objects. Quantitative measures for the importance of the proposed features integration for detecting camouflaged objects are provided in Table 1. It shows that the average object detection accuracy [50] of different considered sequences using different features and their various combinations. This table also highlights that the proposed integration of features from multi-cue, provides better results.

different features and their combinations							
Sequences	C	S	T	CS	CT	TS	CST
*Clip*152	0.9800	0.9589	0.9819	0.9841	0.9869	0.9732	0.9908
*Clip*730	0.9769	0.9200	0.9719	0.9121	0.9779	0.8469	0.9779
*Clip*187	0.6657	0.6717	0.6707	0.9004	0.8278	0.9699	0.9745

Table 1 Average object detection accuracy based on various features. C: color; S: shape; T: texture; CS: color and shape; CT: color and texture; TS: texture and shape; CST: color, shape and texture; green: best among individual features; pink: best among combination of two features; red: best among all individual features and their combinations.

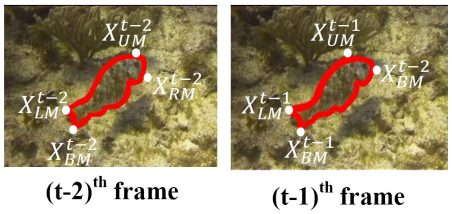

Fig. 7 estimation of rough motion between $(t-2)^{th}$ and $(t-1)^{th}$ frames.

2.2 Rough Estimation of Object Motion

In this article, object motion between two consecutive frames is roughly estimated in a similar way as discussed in [51]. Suppose, contours of the camouflaged object in two consecutive ($(t-2)^{th}$ and $(t-1)^{th}$) frames are available and motion of the camouflaged object between $(t-1)^{th}$ and t^{th} frames need to be estimated. Let $\mathbf{X}_{BM}^{t-2}$, $\mathbf{X}_{BM}^{t-1}$, $\mathbf{X}_{UM}^{t-2}$, $\mathbf{X}_{UM}^{t-1}$, $\mathbf{X}_{LM}^{t-2}$, $\mathbf{X}_{LM}^{t-1}$, $\mathbf{X}_{RM}^{t-2}$ and $\mathbf{X}_{RM}^{t-1}$ be the bottom most, upper most, left most and right most points on the contours of the object in the $(t-2)^{th}$ and the $(t-1)^{th}$ frames, respectively (see Fig. 7). Motion (M) of the object between these two frames is roughly estimated as:

$$M = \max\{\|\mathbf{X}_{BM}^{t-2} - \mathbf{X}_{BM}^{t-1}\|, \|\mathbf{X}_{UM}^{t-2} - \mathbf{X}_{UM}^{t-1}\|, \|\mathbf{X}_{LM}^{t-2} - \mathbf{X}_{LM}^{t-1}\|, \|\mathbf{X}_{RM}^{t-2} - \mathbf{X}_{RM}^{t-1}\|\}, \quad (3)$$

where $\|.\|$ is Euclidean distance. Since movement of the object is not constant throughout the sequence, motion of the object between the $(t-2)^{th}$ and $(t-1)^{th}$ frames is not similar for the $(t-1)^{th}$ and t^{th} frames. Hence, motion of the object between the $(t-1)^{th}$ and the t^{th} frames is modified as

$$\bar{M} = \gamma * M, \quad (4)$$

where $\gamma \in \mathbb{R}$ is a camera or object deformation parameter.

2.3 Camouflaged Object Detection using Proposed Modified Probabilistic Neural Network based Discriminative Appearance Model

Probabilistic neural network (PNN) [65] developed by Specht, has became an efficient tool for solving many pattern classification and computer vision problems [24, 53, 75] due to its easy, non iterative training process and statistical foundation in Bayesian estimation theory. PNN consists of four (input, pattern, summation and decision) layers with neurons. Pattern layer of PNN consists of all training samples including redundant samples. Inclusion of redundant training samples may lead to a large architecture. The large network structure introduces two problems: (i) high computational cost is required to classify an unknown sample because the amount of computation necessary to classify an unknown sample is proportional to the size of the network [49,71], (ii) due to the large network architecture, classifier is highly biased to the training samples and exhibit poor generalization capacities to the unseen data (i.e. overfitting problem) [5,49,71]. Some algorithms for reduction of redundant training samples have been proposed in literature [7, 49, 58, 71]. In this work, we have also proposed a technique based on motion of the object between two consecutive frames to reduce redundant training samples for classifying unlabeled samples. Here, instead of considering the whole training set, a subset (generated based on motion of object) of training set is considered to classify each unlabeled sample. For different unlabeled samples, different training subsets (consist of equal number of training samples) are generated. As PNN has non iterative training process and consideration of training subset reduces the architecture of modified PNN, the proposed discriminative appearance model takes less computational time than the original PNN to classify the unlabeled samples. Moreover, the proposed modified PNN considers local information instead of global information to classify unlabeled samples, thereby increasing the classification accuracy.

2.3.1 Generation of Training and Testing Samples

To construct an appearance model for both the object and the background, prior knowledge about the label of each pixel (or pattern or sample) can be learned from a training (i.e., target[2]) frame. By convention, the pixels within the contour of the object are termed as positive pixels and pixels outside the contour are treated as negative pixels. Positive and negative pixels in d-dimensional feature space are termed as positive and negative samples, respectively. Training set consists of these positive and negative samples. Fig. 8(a) shows the target frame where the object is bounded by its (red colored) contour.

Test set is generated from the test (i.e., target candidate[3]) frame. All pixels of the test frame in d-dimensional feature space are called test samples. Fig. 8(b) displays the target candidate frame from which the moving object needs to be detected.

In this investigation, to classify each unlabeled sample in the t^{th} frame, instead of considering the whole training set generated from the $(t-1)^{th}$ frame, a subset

[2] In this article, training, target, $(t-1)^{th}$ and previous frame are used interchangeably

[3] In this article, test, target candidate, t^{th} and current frame are used interchangeably

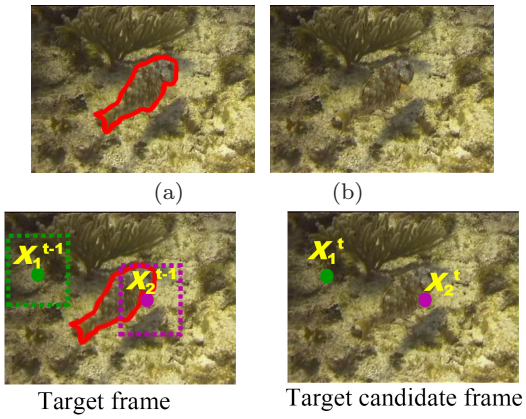

Fig. 8 (a) Target frame; (b) target candidate frame; (c) generation of training subset for each unlabeled sample of Clip152 sequence.

of training set is considered [51]. The training subset for each test sample is generated with the labeled samples within a spatial neighborhood (window) at the corresponding location in the $(t-1)^{th}$ frame of an unlabeled sample in the t^{th} frame. Fig. 8(c) depicts the generation of training subset for each unlabeled sample in the target candidate frame. Here, to classify unlabeled sample, corresponding to pixel $\mathbf{X}_1^t$ in the t^{th} frame, the training subset is generated from the green colored dotted rectangle in the $(t-1)^{th}$ frame. $\mathbf{X}_1^{t-1}$ in the $(t-1)^{th}$ frame is the corresponding pixel of $\mathbf{X}_1^t$ at the t^{th} frame. For different unlabeled samples, different training subsets are generated. A heuristic approach based on motion $(\bar{M})$ of the object is proposed to generate the training subset. The neighborhood (window) size is taken as $\bar{M} \times \bar{M}$.

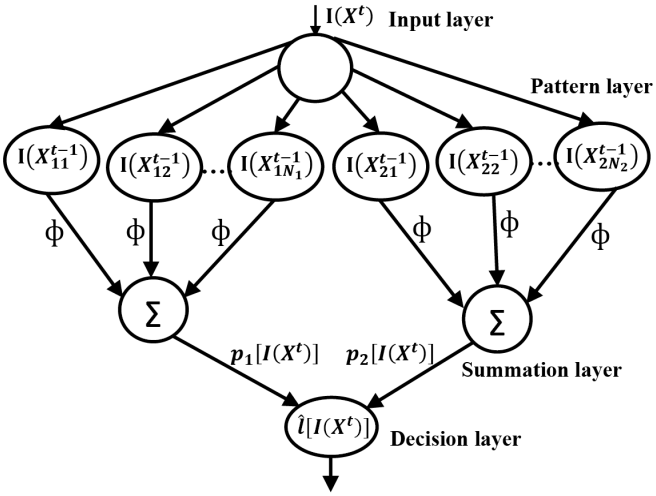

Fig. 9 Architecture of the modified PNN.

Use of local training subset reduces the number of neurons in the pattern layer of the modified PNN. Smaller number of nodes in the pattern layer minimizes the architecture of the modified PNN. Fig. 9 shows the architecture of the modified PNN. It consists of several interconnected neurons organized in successive layers. Input layer does not perform any computation, it only distributes the input patterns to the neurons in the pattern layer. After receiving input (unlabeled) pattern $I(\mathbf{x}^t)$ from the input layer, neuron (corresponding to labeled patterns) $I\left(\mathbf{x}_{ij}^{t-1}\right)$ at the pattern layer computes its output as

$$\phi_{ij}\left[I\left(\mathbf{X}^t\right)\right] = \frac{1}{(2\pi)^{\frac{d}{2}}\sigma^d}\left[e^{-\frac{\left[I(\mathbf{x}^t)-I\left(\mathbf{x}_{ij}^{t-1}\right)\right]^T\left[I(\mathbf{x}^t)-I\left(\mathbf{x}_{ij}^{t-1}\right)\right]}{2\sigma^2}}\right] \quad (5)$$

where d is the dimension of the feature vector representing a pattern, $I\left(\mathbf{X}_{ij}^{t-1}\right)$ is the j^{th} training pattern of the i^{th} class in the $(t-1)^{th}$ frame, $I\left(\mathbf{X}^t\right)$ is the test pattern in the t^{th} frame, σ is the smoothing parameter and $\mathbf{x}_{ij}^{t-1} \in \eta_{\mathbf{x}^t}^t$, where $\eta_{\mathbf{x}^t}^t$ is the temporal neighborhood of $\mathbf{x}^t$.

The neurons at the summation layer compute the maximum likelihood of the unlabeled pattern $I(\mathbf{x}^t)$ being classified into $l_i;\ i = 1,\ 2$ by averaging the output of all neurons which belong to the same class. Therefore

$$p_i\left[I\left(\mathbf{X}^t\right)\right] = \frac{1}{N_i}\sum_{j=1}^{N_i}\phi_{ij}\left[I\left(\mathbf{X}^t\right)\right], \quad (6)$$

where N_i denotes the total number of training samples of class $l_i;\ i = 1,\ 2$. The neuron at the decision layer classifies the pattern $I(\mathbf{x}^t)$ according to Bayes' decision rule based on output of all neurons in the summation layer. Thus, class label of the pattern $I(\mathbf{x}^t)$ is estimated as

$$\hat{l}\left[I\left(X^t\right)\right] = \max\left\{p_i\left[I\left(X^t\right)\right]\right\},\ i = 1, 2. \quad (7)$$

All pixels of the t^{th} frame are thus classified as either object or background; hence, detects the object.

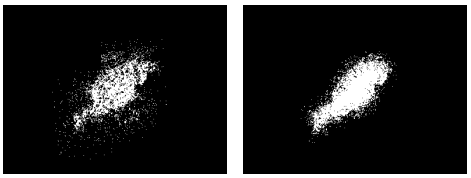

Fig. 10 Detection of camouflaged object in the target candidate frame of Clip152 sequence using (a) PNN (considering whole training set) and (b) the proposed modified PNN (considering local training subset).

Fig. 10(a) shows the object detection result of Clip152 sequence using PNN with consideration of all training

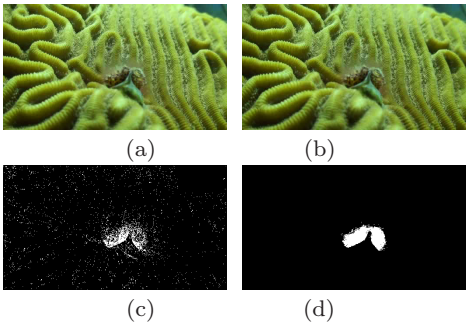

Fig. 11 (a) Target frame; (b) target candidate frame. Detection of camouflaged object in the target candidate frame of Clip730 sequence using (c) PNN (considering whole training set) and (d) the proposed modified PNN (considering local training subset).

samples and it takes 2.77 seconds to detect object in a single frame. Fig. 10(b) displays the detected object of Clip152 sequence using the modified PNN with consideration of local training subset and it takes 0.06 seconds to detect the object in a single frame. Similarly, Figs. 11(c) and (d) display the detected camouflaged object in the target candidate frame of Clip730 sequence with consideration of all training samples and local training subset; and take 4.46 and 0.07 seconds for executing a single frame, respectively. Both these examples highlight the efficiency of the proposed discriminative appearance model by modifying PNN for detecting the camouflaged objects in the target candidate frame. Table 2 shows the detection accuracy based on (whole and local) training set. This table also highlights that the modified PNN (consideration of local training set) produces better result than PNN (consideration of whole training set) in camouflaged condition. Description of these datasets are given in Table 3. To extract the contour of the camouflaged object or to track such an object, a fuzzy energy based active contour with global and local information is proposed. The proposed fuzzy energy based active contour is evolved with the detected object by the modified PNN as an initialization. Object tracking using the proposed fuzzy energy based active contour model is explained in the following subsection.

Sequences	All training patterns	Selected training patterns
*Clip*152	0.9641	0.9820
*Clip*730	0.9687	0.9939

Table 2 Average (object detection) accuracy based on training patterns. Red: indicates best results.

2.4 Camouflaged Object Tracking using the Proposed Global and Local Fuzzy Energy based Active Contour Model

2.4.1 Existing Global Fuzzy Energy based Active Contour Model

Fuzzy active contour model proposed by Krinidis and Chatzis [37] is formulated below.

Let an image be $I(\mathbf{X}) : \Omega \rightarrow \Re^d$, where $\Omega \subset \Re^2$ is the image domain and d is the dimension of feature vector $I(\mathbf{X})$. Let C be a closed contour in the domain Ω which separates Ω into two regions: $\Omega_1 = inside\,(C)$ and $\Omega_2 = outside\,(C)$. The general form of energy function which approximates the given image $I(\mathbf{X})$ by two regions over Ω, defined in [37] is given as

$$\begin{aligned} F\,(C, c_1, c_2, u) &= \lambda_1 \beta \int\limits_{\Omega} [u\,(\mathbf{X})]^m \left\| I(\mathbf{X}) - c_1 \right\|^2 d\mathbf{X} \\ &+ \lambda_2 \beta \int\limits_{\Omega} [1 - u\,(\mathbf{X})]^m \left\| I(\mathbf{X}) - c_2 \right\|^2 d\mathbf{X} \\ &+ \mu . L\,(C)\,; \end{aligned} \tag{8}$$

where $c_1 \in \Re^d$ and $c_2 \in \Re^d$ (depending on C) are the average prototypes of the regions for the given image inside and outside the contour C. The membership function $u\,(\mathbf{X}) \in [0, 1]$ is the membership of a pixel $\mathbf{X}$ for belonging to the inside of C. $m > 1$ is a weight exponent which controls the degree of 'fuzziness' of each membership value.

2.4.2 Proposed Global and Local Fuzzy Energy based Active Contour Model

In this article, we proposed a new fuzzy energy function by incorporating local energy term in the existing global fuzzy energy based active contour model [37] defined in Eq.(8). Basically, local energy term is calculated based on local spatial constraint and local feature constraint. The proposed fuzzy energy based function that takes both global and local information to track the contour of the detected object. After transforming t^{th} frame into the normalized d-dimensional feature space, we have $I(\mathbf{X}^t) : \Omega \rightarrow \Re^d$, where $\Omega \subset \Re^2$ is the domain of the image frame and d is the dimension of feature vector $I(\mathbf{X}^t)$. Let C be a closed contour in the domain Ω which separates Ω into two regions: $\Omega_1 = inside\,(C)$ and $\Omega_2 = outside\,(C)$. The general form of the proposed energy function when t^{th} frame $I(\mathbf{X}^t)$ is approx-

imated by two regions over Ω, is

$$
\begin{aligned}
F\left(C, c_1, c_2, u\right) &= \lambda_1 \beta \int_{\Omega} \left[u\left(\mathbf{X}^t\right)\right]^m \left\|I(\mathbf{X}^t) - c_1\right\|^2 d\mathbf{X}^t \\
&+ \lambda_2 \beta \int_{\Omega} \left[1 - u\left(\mathbf{X}^t\right)\right]^m \left\|I(\mathbf{X}^t) - c_2\right\|^2 d\mathbf{X}^t \\
&+ \lambda_1 \left(1-\beta\right) \int_{\Omega} \left[u\left(\mathbf{X}^t\right)\right]^m h_1 \; d\mathbf{X}^t \\
&+ \lambda_2 \left(1-\beta\right) \int_{\Omega} \left[1 - u\left(\mathbf{X}^t\right)\right]^m h_2 \; d\mathbf{X}^t \\
&+ \mu . L\left(C\right);
\end{aligned} \tag{9}
$$

with

$$
\begin{aligned}
h_1 &= \int_{\Omega} W_{\mathbf{X}^t\mathbf{Y}^t} \left[1 - u\left(\mathbf{Y}^t\right)\right]^m \left\|I(\mathbf{Y}^t) - c_1\right\|^2 d\mathbf{Y}^t, \\
h_2 &= \int_{\Omega} W_{\mathbf{X}^t\mathbf{Y}^t} \left[u\left(\mathbf{Y}^t\right)\right]^m \left\|I(\mathbf{Y}^t) - c_2\right\|^2 d\mathbf{Y}^t,
\end{aligned}
$$

where $c_1 \in \Re^d$ and $c_2 \in \Re^d$ (depending on C) are the average prototypes of the regions for the t^{th} frame inside and outside the contour C. The membership function $u\left(\mathbf{X}^t\right) \in [0,1]$ is the membership of a pixel $\mathbf{X}^t$ for belonging to inside of C. $m > 1$ is a weight exponent which controls the degree of 'fuzziness' of each membership value. The term $I(\mathbf{Y}^t)$ represents the feature values of a pixel $\mathbf{Y}^t$ in a spatial neighborhood of a pixel $\mathbf{X}^t$. $W_{\mathbf{X}^t\mathbf{Y}^t}$ is the weight of $\mathbf{Y}^t$ pixel in a local neighborhood of pixel $\mathbf{X}^t$. $\lambda_1 > 0$ and $\lambda_2 > 0$ are two fixed parameters; $0 \leq \beta \leq 1$ is a constant to control the influence of both the global energy and local energy. $\mu \geq 0$ is the length parameter of the curve C and it can be chosen by the user. Effect of the length parameter for the images without any artifacts was briefly discussed in [28, 57]. This parameter is not important for such kind of images. However, in case of noisy images, the length parameter can be useful and is briefly discussed in [37, 44].

Here, the weight $W_{\mathbf{X}^t\mathbf{Y}^t}$ depends on both the local spatial constraint and local feature constraint. For each pixel $\mathbf{X}^t \in \Re^2$, the local spatial constraint reflects the damping extent of neighbors with the spatial distances from the central pixel and is defined as

$$
W^{SC}_{\mathbf{X}^t\mathbf{Y}^t} = \frac{1}{1 + d_{\mathbf{X}^t\mathbf{Y}^t}} \tag{10}
$$

with $d_{\mathbf{X}^t\mathbf{Y}^t} = \|\mathbf{X}^t - \mathbf{Y}^t\|, \mathbf{Y}^t \in \eta_{\mathbf{X}^t}$, where $\eta_{\mathbf{X}^t}$ is the spatial neighborhood (local window) of $\mathbf{X}^t$. The spatial constraint ensures the influence of pixels within the local window. It can be changed according to their distances from the central pixel. With the help of spatial constraint, more local information is incorporated in the proposed energy model.

The local feature constraint is defined as

$$
W^{FC}_{\mathbf{X}^t\mathbf{Y}^t} = \exp\left\{ \frac{-\left\|I(\mathbf{X}^t) - I(\mathbf{Y}^t)\right\|^2}{\sum\limits_{\mathbf{Y}^t \in \eta_{\mathbf{X}^t}} \|I(\mathbf{X}^t) - I(\mathbf{Y}^t)\|^2} \right\}, \tag{11}
$$

where $I(\mathbf{X}^t)$ is the d-dimensional feature vector of the central pixel $\mathbf{X}^t$ within a spatial local window and $I(\mathbf{Y}^t)$ is the d-dimensional feature vector of $\mathbf{Y}^t$ pixels in the same window. $\eta_{\mathbf{X}^t}$ is the neighborhood of pixel $\mathbf{X}^t$. The denominator is a function of local density surrounding the central pixel and its value reflects the feature homogeneity degree of that local window. When its value is small, the local window is more homogeneous and vice versa. Eq. (11) indicates that when the feature vector $I(\mathbf{Y}^t)$ is close to $I(\mathbf{X}^t)$, $W^{FC}_{\mathbf{X}^t\mathbf{Y}^t}$ is large and vice versa. The value of $W^{FC}_{\mathbf{X}^t\mathbf{Y}^t}$ can be changed with different feature values of the pixels over a frame and thus it reflects the damping extent in the feature values. Now, the weight $W_{\mathbf{X}^t\mathbf{Y}^t}$ based on both the local spatial constraint and local feature constraint is defined as

$$
W_{\mathbf{X}^t\mathbf{Y}^t} = W^{SC}_{\mathbf{X}^t\mathbf{Y}^t} * W^{FC}_{\mathbf{X}^t\mathbf{Y}^t}. \tag{12}
$$

The energy function (in Eq. (9)) can be minimized when the contour C is exactly on the object boundary and c_1 and c_2 optimally approximate the t^{th} frame into two regions inside and outside the contour C, respectively. To obtain the entire object boundary, a contour C has to be found which minimizes the proposed energy function given in Eq. (9) over all pixels $\mathbf{X}^t \in \Omega$. In addition, sometimes to smooth the contour C, one penalty term i.e., length $L(C)$ of the contour C is considered for the proposed energy function.

The energy function given in Eq. (9) will be minimized when $C = C_O$, i.e.,

$$
C_O = \arg\min_{C} F\left(C, c_1, c_2, u\right). \tag{13}
$$

Therefore, the curve C_O is the extracted contour in the t^{th} frame and the object is tracked with the extracted contour in the t^{th} frame. Figs. 12 and 13 show the tracking results of camouflaged object in the t^{th} frame of Clip152 and Clip730 sequences, respectively, using the proposed fuzzy energy based active contour.

Fig. 12 Camouflaged object is tracked in the target candidate frame of Clip152 sequence using the proposed fuzzy energy based active contour.

2.4.3 Pseudo Level Set Formulation

The proposed fuzzy energy function is formulated using a pseudo level set formulation as considered in [37] and [56] based on the membership values. The curve $C \subset \Omega$

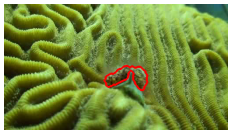

Fig. 13 Camouflaged object is tracked in the target candidate frame of Clip730 sequence using the proposed fuzzy energy based active contour.

is implicitly represented by the pseudo zero level set of Lipschitz function $u(\mathbf{X}^t) : \Omega \to \Re$, such that

$$\begin{cases} C = \left\{\mathbf{X}^t \in \Omega : u\left(\mathbf{X}^t\right) = 0.5\right\}, \\ inside\left(C\right) = \left\{\mathbf{X}^t \in \Omega : u\left(\mathbf{X}^t\right) > 0.5\right\}, \\ outside\left(C\right) = \left\{\mathbf{X}^t \in \Omega : u\left(\mathbf{X}^t\right) < 0.5\right\}. \end{cases} \tag{14}$$

Here, it is noted that the regularization or the penalty term of the proposed energy function $F(C, c_1, c_2, u)$ given in Eq. (9) is $L(C) = \int\limits_{\Omega} \left|\nabla H\left(u\left(\mathbf{X}^t\right) - 0.5\right)\right| d\mathbf{X}^t$, where $H\left(s\right)$ is a heaviside function [56]. Therefore, the energy function in Eq. (9) can be rewritten as

$$\begin{aligned} &F\left(C, c_1, c_2, u\right) = \lambda_1 \beta \int\limits_{\Omega} \left[u\left(\mathbf{X}^t\right)\right]^m \left\|I(\mathbf{X}^t) - c_1\right\|^2 d\mathbf{X}^t \\ &+\lambda_2 \beta \int\limits_{\Omega} \left[1 - u\left(\mathbf{X}^t\right)\right]^m \left\|I(\mathbf{X}^t) - c_2\right\|^2 d\mathbf{X}^t \\ &+\lambda_1 \left(1-\beta\right) \int\limits_{\Omega} \left[u\left(\mathbf{X}^t\right)\right]^m h_1 \; d\mathbf{X}^t \\ &+\lambda_2 \left(1-\beta\right) \int\limits_{\Omega} \left[1 - u\left(\mathbf{X}^t\right)\right]^m h_2 \; d\mathbf{X}^t \\ &+\mu \int\limits_{\Omega} \left|\nabla H\left(u\left(\mathbf{X}^t\right) - 0.5\right)\right| d\mathbf{X}^t. \end{aligned} \tag{15}$$

The values of u for the pixels located inside the contour C are different from the corresponding values for the pixels located outside the contour, when the energy function is minimized. However, the values of u for the pixels located inside the contour C are similar. This is the same for the pixels located outside the contour C.

Now keeping u fixed and minimizing the energy function $F\left(C, c_1, c_2, u\right)$ (in Eq. (15)) with respect to c_1 and c_2, we get the following equations:

$$\begin{aligned} &\int\limits_{\Omega} \left[u\left(\mathbf{X}^t\right)\right]^m \left[I\left(\mathbf{X}^t\right) - c_1\right] d\mathbf{X}^t = 0 \\ &\Rightarrow c_1 = \frac{\int\limits_{\Omega} \left[u(\mathbf{X}^t)\right]^m I(\mathbf{X}^t) d\mathbf{X}^t}{\int\limits_{\Omega} \left[u(\mathbf{X}^t)\right]^m d\mathbf{X}^t}, \end{aligned} \tag{16}$$

and

$$\begin{aligned} &\int\limits_{\Omega} \left[1 - u\left(\mathbf{X}^t\right)\right]^m \left[I\left(\mathbf{X}^t\right) - c_2\right] d\mathbf{X}^t = 0 \\ &\Rightarrow c_2 = \frac{\int\limits_{\Omega} \left[1-u(\mathbf{X}^t)\right]^m I(\mathbf{X}^t) d\mathbf{X}^t}{\int\limits_{\Omega} \left[1-u(\mathbf{X}^t)\right]^m d\mathbf{X}^t}. \end{aligned} \tag{17}$$

Again, keeping c_1 and c_2 fixed and minimizing the energy function $F\left(C, c_1, c_2, u\right)$ (given in Eq.(15)) with respect to $u(\mathbf{X}^t)$, we get

$$\begin{aligned} &\lambda_1 \beta m \left[u\left(\mathbf{X}^t\right)\right]^{m-1} \left\|I(\mathbf{X}^t) - c_1\right\|^2 \\ &-\lambda_2 \beta m \left[1 - u\left(\mathbf{X}^t\right)\right]^{m-1} \left\|I(\mathbf{X}^t) - c_2\right\|^2 \\ &+\lambda_1 \left(1-\beta\right) m \left[u\left(\mathbf{X}^t\right)\right]^{m-1} h_1 \\ &-\lambda_2 \left(1-\beta\right) m \left[1 - u\left(\mathbf{X}^t\right)\right]^{m-1} h_2 = 0 \\ &\Rightarrow u\left(\mathbf{X}^t\right) = \frac{1}{1+\left(\frac{\lambda_1\left\{\beta\left\|I(\mathbf{X}^t)-c_1\right\|^2+(1-\beta)h_1\right\}}{\lambda_2\left\{\beta\left\|I(\mathbf{X}^t)-c_2\right\|^2+(1-\beta)h_2\right\}}\right)^{\frac{1}{m-1}}}, \end{aligned} \tag{18}$$

where h_1, h_2 are similar as defined in Eq. (9).

For simplicity, without loss of generality, the above minimization (Eq. (18)) has been done without considering the length term (i.e., $\mu = 0$).

2.4.4 Convexity of the Proposed Energy Model

The contour is iteratively evolved with an initialization (object detection result of the modified PNN). When the energy function defined in Eq. (15) is minimum, the optimal contour is obtained. If the energy function is convex, then it is easy to find the global optimal solution (contour) with an iterative way. Therefore, in this section, we will prove that the proposed energy function F in Eq. (15) is convex with respect to u.

Proof is given in Appendix A.

2.4.5 Numerical Approximation

The proposed energy function (given in Eq. (15) as a minimization problem) can be solved by the gradient descent approach which is derived from the Euler-Lagrange equation [20]. But it is slow for convergence [37]. In this article, a fast numerical approach proposed by Song and Chen [64] and developed by Krinidis and Chatzis [37], is used. Instead of solving the Euler-Lagrange equation, this method calculates and verifies whether the energy decreases when the membership value of any arbitrary pixel on the t^{th} frame changes or vice versa.

Now for a pixel $\mathbf{X}^t \in \Omega$ of the t^{th} frame, the feature value of the pixel $\mathbf{X}^t$ is I_o and the corresponding degree of membership is u_o. Assume that the degree of membership of the pixel $\mathbf{X}^t$ is changed to a new value u_n which is calculated using Eq. (18). Let ΔF be the difference between the new and old energies when the degree of membership of pixel $\mathbf{X}^t$ is changed. Then ΔF (detail derivation is given in Appendix B) is calculated

as follows:

$$
\begin{aligned}
&\Delta F = \lambda_1 \beta S_1 a_1 \|I_o - c_1\|^2 + \lambda_2 \beta S_2 a_2 \|I_o - c_2\|^2 \\
&-2\lambda_1 (1-\beta) S_1 \|I_o - c_1\| b_1 \\
&+\lambda_1 (1-\beta) g_1 \left[\|c_1 + S_1 (\|I_o - c_1\|)\|^2 - \|c_1\|^2\right] \\
&+\lambda_1 (1-\beta) \left([u_n]^m - [u_o]^m\right) \\
&\left\{\sum_{\Omega} W_{o\mathbf{Y}^t} \left[1 - u\left(\mathbf{Y}^t\right)\right]^m \|I(\mathbf{Y}^t) - c_1 - S_1 (\|I_o - c_1\|)\|^2\right\} \\
&+\lambda_1 (1-\beta) \left([u_n]^m - [u_o]^m\right) \\
&\left\{\sum_{\Omega} W_{o\mathbf{Y}^t} \left[1 - u\left(\mathbf{Y}^t\right)\right]^m \|I_o - c_1\|^2 [1 - S_1]^2\right\} \\
&-2\lambda_2 (1-\beta) S_2 \|I_o - c_2\| b_2 \\
&+\lambda_2 (1-\beta) g_2 \left[\|c_2 + S_2 (\|I_o - c_2\|)\|^2 - \|c_2\|^2\right] \\
&+\lambda_2 (1-\beta) \left[(1-u_n)^m - (1-u_o)^m\right] \\
&\left\{\sum_{\Omega} W_{o\mathbf{Y}^t} \left[u\left(\mathbf{Y}^t\right)\right]^m \|I(\mathbf{Y}^t) - c_2 - S_2 (\|I_o - c_2\|)\|^2\right\} \\
&+\lambda_2 (1-\beta) \left[(1-u_n)^m - (1-u_o)^m\right] \\
&\left\{\sum_{\Omega} W_{o\mathbf{Y}^t} \left[u\left(\mathbf{Y}^t\right)\right]^m \|I_o - c_2\|^2 [1 - S_2]^2\right\},
\end{aligned}
\tag{19}
$$

where

$$
\begin{aligned}
&a_1 = \sum_{\Omega} \left[u\left(\mathbf{X}^t\right)\right]^m,\ a_2 = \sum_{\Omega} \left[1 - u\left(\mathbf{X}^t\right)\right]^m, \\
&S_1 = \frac{[u_n]^m - [u_o]^m}{\sum_{\Omega} [u(\mathbf{X}^t)]^m + [u_n]^m - [u_o]^m}, \\
&S_2 = \frac{(1-u_n)^m - (1-u_o)^m}{\sum_{\Omega} [1-u(\mathbf{X}^t)]^m + (1-u_n)^m - (1-u_o)^m}, \\
&b_1 = \sum_{\Omega} \left[u\left(\mathbf{X}^t\right)\right]^m \left\{\sum_{\Omega} W_{\mathbf{X}^t\mathbf{Y}^t} \left[1 - u\left(\mathbf{Y}^t\right)\right]^m I(\mathbf{Y}^t)\right\}, \\
&b_2 = \sum_{\Omega} \left[1 - u\left(\mathbf{X}^t\right)\right]^m \left\{\sum_{\Omega} W_{\mathbf{X}^t\mathbf{Y}^t} \left[u\left(\mathbf{Y}^t\right)\right]^m I(\mathbf{Y}^t)\right\}, \\
&g_1 = \sum_{\Omega} \left[u\left(\mathbf{X}^t\right)\right]^m \left\{\sum_{\Omega} W_{\mathbf{X}^t\mathbf{Y}^t} \left[1 - u\left(\mathbf{Y}^t\right)\right]^m\right\}, \\
&g_2 = \sum_{\Omega} \left[1 - u\left(\mathbf{X}^t\right)\right]^m \left\{\sum_{\Omega} W_{\mathbf{X}^t\mathbf{Y}^t} \left[u\left(\mathbf{Y}^t\right)\right]^m\right\}.
\end{aligned}
$$

2.5 Online Update to Handle Drift Problem

To capture the changes due to both camera and object motions, the proposed modified PNN based discriminative appearance model needs to be updated. In this work, after tracking the object in the t^{th} frame, new training (samples) information generated from the t^{th} frame is used to update the proposed discriminative model and to detect and track the object in the next $(t+1)^{th}$ frame. Since every time, the proposed discriminative appearance model is updated with new information, it is able to reduce the propagation of drift.

2.6 Computational Complexity

Let N be the total number of patterns (corresponding to pixels) in the t^{th} frame. Let the cost for calculating HOG feature for each pixel be f_{hog}. Therefore, total cost for calculating HOG of each frame is $N * f_{hog}$. Now

$$N * f_{hog} = N * B_{hog} * W_{hog} + f_{n_1},$$

where B_{hog} is the number of considered histogram bins and W_{hog} is the considered window size. Again let the cost for calculating LTP feature for each pixel be f_{ltp}. Therefore, total cost for generating LTP of a frame is $N * f_{ltp}$. Now

$$N * f_{ltp} = N(f_a * W_{ltp} + f_{n_2}),$$

where W_{ltp} is the considered window size. Therefore, let the total cost required to generate 13-dimensional feature vectors for a frame be $f_{feature}$. We have

$$f_{feature} = N * f_{hog} + N * f_{ltp} + f_{n_3},$$

where f_{n_3} is a constant cost. To estimate the motion of the object between the $(t-1)^{th}$ and the t^{th} frames using Eqs. (3) and (4), they need constant costs f_{n_4} and f_{n_5}, respectively. To classify each test pattern in the t^{th} frame, let it require f_{pnn} cost. Then we have

$$f_{pnn} = N_1 * f_{n_6} + N_1 * f_{n_7} + f_{n_8},$$

where N_1 is the number of training samples and $N_1 << N$. Therefore, total cost required to detect an object in the t^{th} frame is

$$N * f_{pnn} = N(N_1 * f_{n_6} + N_1 * f_{n_7} + f_{n_8}).$$

In the proposed fuzzy active contour model, let W be the size of the considered neighborhood and T be the total number of iterations required to converge, then the total cost required for fuzzy active contour is

$$f_{facm} = N * W * T * f_b + f_{n_9}.$$

Therefore, total cost required for the proposed tracking algorithm is

$$
\begin{aligned}
&f_t = f_{feature} + N * f_{pnn} + f_{facm} + f_{n_4} + f_{n_5} \\
&= N * f_{hog} + N * f_{ltp} + f_{n_3} \\
&+N(N_1 * f_{n_6} + N_1 * f_{n_7} + f_{n_8}) \\
&+N * W * T * f_b + f_{n_9} + f_{n_4} + f_{n_5} \\
&= N * B_{hog} * W_{hog} + f_{n_1} + N(f_a * W_{ltp} + f_{n_2}) + f_{n_3} \\
&+N(N_1 * f_{n_6} + N_1 * f_{n_7} + f_{n_8}) \\
&+N * W * T * f_b + f_{n_9} + f_{n_4} + f_{n_5} \\
&\leq N^2, N \gg N_1 \text{ and } N \gg T.
\end{aligned}
$$

For all the experiments, B_{hog}, W_{hog}, W_{ltp} and W are constants. Therefore, time complexity of the proposed tracking algorithm is

$$f_t = \mathrm{O}\left(N^2\right).$$

Here we also provide the proposed tracking method in an algorithmic form.

Algorithm 1 : Proposed Algorithm

Input: $I(\mathbf{X}^{t-2})$ and $I(\mathbf{X}^{t-1})$ with object contours $C(\mathbf{X}^{t-2})$ and $C(\mathbf{X}^{t-1})$.
Output: Contour $C(\mathbf{X}^t)$ in the t^{th} frame.

for(t=3 to end of the sequence)

1: Transform both $I(\mathbf{X}^{t-1})$ and $I(\mathbf{X}^t)$ into d-dimensional feature space.
2: Calculate motion ($\bar{M}$) of the object between the $(t-2)^{th}$ and the $(t-1)^{th}$ frames using Eqs. (3) and (4).
3: Detect object in the t^{th} frame using the proposed modified PNN.
4: Extract contour $C(\mathbf{X}^t)$ of the object in the t^{th} frame using the proposed fuzzy active contour model.
(i): For initial partition, set up $u(\mathbf{X}^t) > 0.5$ for one part (detected object region) and $u(\mathbf{X}^t) < 0.5$ for the other part (i.e., outside the detected object region).
(ii): Compute $c_1(\mathbf{X}^t)$ and $c_2(\mathbf{X}^t)$ using Eqs.(16) and (17).
(iii): Assume that feature value of the current pixel $\mathbf{X}^t$ is $I_o(\mathbf{X}^t)$ and $u_o(\mathbf{X}^t)$ is its degree of membership value. Then the new degree of membership value $u_n(\mathbf{X}^t)$ is calculated by using Eq. (18) for the current pixel $\mathbf{X}^t$. The difference between new and old energies ΔF is calculated by using Eq. (19).
If $\Delta F < 0$, then $u_o(\mathbf{X}^t)$ is changed by $u_n(\mathbf{X}^t)$, otherwise keep the old value $u_o(\mathbf{X}^t)$.
(iv): Repeat step (iii) using Jacobi iteration to calculate total energy F for the whole t^{th} frame.
(v): Repeat steps (ii)-(iv) till the total energy F remains unchanged.

end

3 Experimental Results and Analysis

In this section, the experimental setups and analysis (both quantitative and qualitative) of results are presented.

3.1 Experimental Setups

We utilized 8 bin HOG, LTPL and LTPU textural features extracted only on the lightness L component of CIELab color space. Here, HOG is 8 dimensional feature vector, color is 3 dimensional feature vector, each of LTPL and LTPU is 1 dimensional feature vector. Therefore, dimension of the required feature vector (combination of color (3), texture (2) and shape (8)) is 13. In all experiments, we set W_{hog}=5, W_{ltp}=3 and W=5. To collect the training set in the initialization step, contours of the target in the 1st and 2nd frames are located by manually cropping. The detected object using the proposed modified PNN in the t^{th} frame is considered to initialize the fuzzy active contour model. Here, camera or object deformation parameter γ is experimentally set to 15 for all experiments. The smoothing parameter σ in PNN is considered in the range $[0.1, 5.0]$. Parameters λ_1 and λ_2 both are set to 1 and β within the range $[0, 1]$. All simulations have been done on a machine with Intel(R) Core(TM)i3 CPU 3.20 GHz, 4.0 GB RAM and fedora operating system.

The proposed algorithm is evaluated on 200 (50 sequences from Visual Tracker Benchmark[4], 100 sequences from Reef Video Clip Database[5], 30 sequences from ALOV++[6] and 20 sequences from VOT2015 Challenge[7]) challenging video sequences. These sequences include most challenging factors in visual tracking like fully or partially camouflaged object, complex background, illumination variation, fast motion, large variation in scale, motion blur, rotation, non-rigid object deformation, partial or full occlusion, low contrast, etc. Due to the page constraint, details about some of the considered video sequences are given in Table 3. The tracking results obtained using the proposed method were compared with recent popular existing tracking algorithms: DFT[8], ASLA[9], MTT[10], SCM[11], SPT[12], KCF[13] and two camouflaged object tracking algorithms: weighted region consolidation (WRC) [31] and optical flow and Kalman filter (OFKF) technique [30]. Here, the proposed method provides object contour (boundary) whereas all existing considered techniques (except WRC) use rectangular trackers. Therefore, to make a fair comparison between the proposed method and all existing considered techniques, rectangular tracker is used with the contour information of the proposed method. However, due to page constraint, results of some (30) sequences are provided in this article. More results (obtained by WRC and OFKF techniques) can be found in the supplementary material.

3.2 Evaluation Methodology

In this article, precision plot, success plot [3,29,73], average center location error and average tracking accuracy (ATA)[36] are considered to quantitatively evaluate the performance of the proposed algorithm for tracking single object. In case of multiple objects tracking, multiple object tracking accuracy (MOTA) and multiple object tracking precision (MOTP) [36] are also considered for quantitative analysis.

[4] http://cvlab.hanyang.ac.kr/tracker_benchmark/indexhtml
[5] http://www.reefvid.org/
[6] http://crcv.ucf.edu/data/ALOV++/
[7] http://www.votchallenge.net/vot2015/dataset.html
[8] http://people.cs.umass.edu/~lsevilla/20trackingDF.html
[9] http://faculty.ucmerced.edu/mhyang/project/cvpr12_jia_project.htm
[10] http://sites.google.com/site/zhangtianzhu2012/publications
[11] http://faculty.ucmerced.edu/mhyang/project/cvpr12_scm.htm
[12] http://www.umiacs.umd.edu/~fyang/spt.html
[13] http://home.isr.uc.pt/~henriques/circulant/

Sequences	frame resolution	total number of frames
bmx	1280X692	76
Butterfly	640X480	151
Crossing	1210X681	131
Iceskate	480X270	661
Octopus	1280X270	291
Sphere	480X360	201
Light23	480X360	238
specularity8	1280X720	119
Shape14	1280X720	299
Motionc1	640X480	196
Confusion35	720X576	109
Low contrast13	1920X1080	421
Moving camera15	854X480	250
Zooming camera25	1920X1080	120
Clip730	512X288	453
Clip152	384X288	198
Clip187	384X288	407
Clip284	384X288	694
Clip442	384X288	1182
Clip498	384X288	166
Clip233	384X288	89
Clip790	360X288	186
Clip796	360X288	1781
Clip249	384X288	183
Trans	640X332	124
Faceocc1	352X288	892
Carscale	640X272	252
Doll	400X300	3872
Jogging	352X288	307
Singer1	624X352	351
Trellis	320X240	569

Table 3 Details about some of the considered sequences.

3.2.1 Precision Plot

Center location error [36] is defined as the Euclidean distance between the center location of the tracked target and the ground truth. Then the average center location error over all the frames of a sequence is considered to summarize the overall performance for that sequence. However, when the tracker loses the target, the output location can be random and the average center location error may be unable to measure the tracking performance correctly [3, 73]. Recently, the precision plot [3, 29, 73] has been considered to measure the overall tracking performance. It shows the percentage of frames whose estimated location is within the given threshold value (with respect to the ground truth). In this article, the threshold value is set to 20 pixels [3,73].

3.2.2 Success Plot

Another evaluation metric is the bounding box (area) overlap. For a given tracked bounding box A and the ground truth bounding box B, the overlap score is defined as $S = \frac{|A \cap B|}{|A \cup B|}$, where $\cap$ and $\cup$ represent the intersection and union of two regions, respectively and $|.|$ denotes the number of pixels in the region. To measure the performance of an algorithm on a sequence of frames, we count the number of successful frames whose overlap score S is larger than the given threshold value. The success plot shows the ratios of successful frames at the thresholds varied from 0 to 1. Success rate value at a specific threshold (e.g., 0.5) may not always be the representative for evaluating tracker performance [73]. Instead of that, area under curve (AUC) [73] of each success plot is considered to evaluate the performance of the tracking algorithms.

3.3 Quantitative Analysis

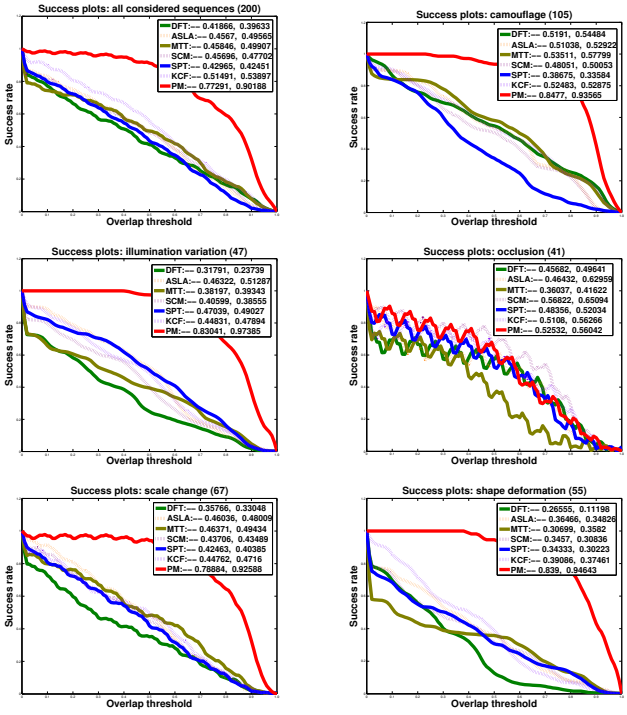

Fig. 14 Each plot corresponds to one-pass evaluation(OPE). In the legend of success plots, the first value is AUC score and the last one is the success rate value at threshold 0.5.

The overall performances of the proposed method and all other existing techniques are summarized by the success and precision plots as shown in Figs. 14 and 15, respectively. For success plots, AUC score is used to summarize the performances of different algorithms, while for precision plots, center location error at threshold value (20) is considered. In the precision plots, the performances of some techniques are different from the performances of algorithms in the success plots. Since success and precision plots are based on different metrics which measure different characteris-

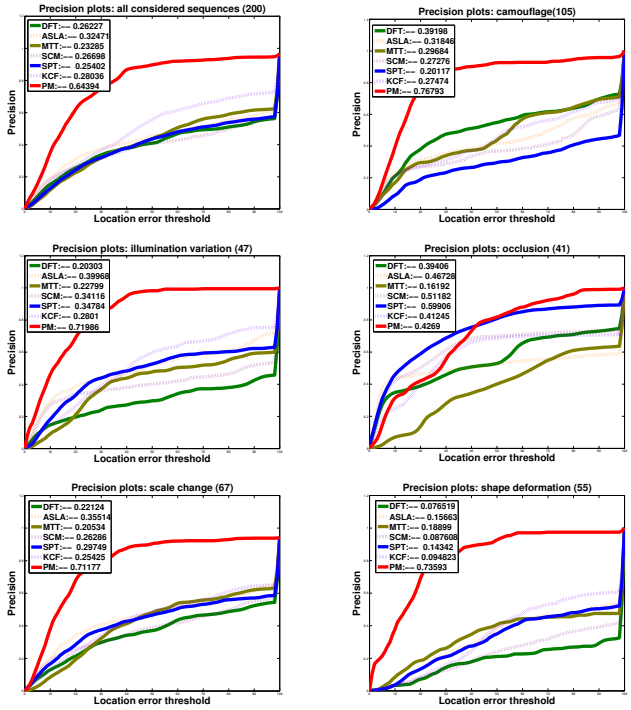

Fig. 15 Each plot corresponds to one-pass evaluation(OPE). In the legend of precision plots, the value indicates precision value at threshold (20 pixels).

tics of the trackers. However, AUC score of the success plot measures the overall performance which is more accurate than the center location error at threshold value of the precision plot [73]. In this article, performances of different algorithms are analyzed based on success plots; however the precision plots can be considered as auxiliary.

From the success plots of all the considered (200) sequences, it is seen that the average performance of KCF is better than all other existing (SCM, SPT, DFT, ASLA and MTT) techniques. This is due to the use of robust appearance model (circulant structure) and update mechanism. ASLA, SCM and MTT have similar (almost equal) performance. Sparse representations are considered in all these techniques. On the other hand, SPT outperforms DFT by 2.5% but below KCF by 19%. However, the proposed method performs better than all existing techniques. Tables 4 and 5 also highlight similar findings. More plots can be found in supplementary material.

Sequences	DFT	ASLA	MTT	SCM	SPT	KCF	PM
200	0.4129	0.4501	0.4504	0.4501	0.4429	0.5098	0.7750

Table 4 Average Tracking Accuracy (area overlap) of all considered (200) sequences. Red: indicates best value, pink: indicates second best, green: indicates third best.

Sequences	DFT	ASLA	MTT	SCM	SPT	KCF	PM
200	66.715	61.778	69.024	62.366	60.294	40.822	10.441

Table 5 Average center location error of all considered (200) sequences. Red: indicates best value, pink: indicates second best, green: indicates third best.

3.3.1 Quantitative Analysis based on Attributes

Here, the performances of the proposed algorithm and other existing techniques are analyzed based on several attributes like camouflage, illumination variation, occlusion, scale change, shape deformation, background clutter, fast motion, pose change, etc. Due to the page constraint, analysis based on some of them (attributes) are discussed here. In case of camouflage, MTT produces better results than all other existing techniques. SPT produces worst results due to segmentation. However, the proposed method obtains the best results among all existing algorithms. Though SPT works well than other state-of-the-art techniques for sequences having illumination variations, but the proposed method provides the best results. In case of occlusion, ASLA, SCM, MTT all performed better due to sparse representation. Among them, SCM provides better results than ASLA and MTT because it uses hybrid (both generative and discriminative) appearance model based on local sparse representation. However, KCF outperforms others while handling occlusion due to kernelized correlation filter based on discrete Fourier transform which is robust under occlusion. On the other hand, the proposed method is unable to detect and track object under full occlusion. But it produces better results for partial occluded objects. Due to partial occlusion, the AUC shows that the proposed method provides acceptable results under occlusion. On the other hand, MTT outperforms for sequences having objects with large scale variations. Among all these techniques, the proposed method obtains the best results because it extracts contour of the object, so scale change can not create a problem for extracting contours. Tables 6 and 7 display the center location errors and average tracking accuracies of some considered sequences for all techniques. These tables also highlight similar findings.

3.4 Qualitative Analysis

Scale change and Pose variation: We evaluate the performances of all the trackers on sequences where objects undergo large scale and pose changes. First, we compare the performances of trackers in terms of handling large scale variation. Carscale and Doll sequences

Sequences	DFT	ASLA	MTT	SCM	SPT	KCF	PM
bmx	80.931404	74.183272	93.527788	86.425588	57.242464	79.103122	4.420175
Butterfly	39.400818	289.603366	300.665582	189.480262	195.836494	24.302096	4.500000
Crossing	22.658566	138.828635	26.915897	51.428637	35.390508	21.700795	4.374453
Iceskate	39.578972	128.544565	196.458901	132.942693	177.144333	20.487457	20.357091
Octopus	59.626939	46.071459	124.365045	61.708927	94.089470	62.336120	6.670759
Sphere	50.751903	133.314856	152.023315	97.857628	16.831229	19.580526	18.971748
Light	163.502168	17.315019	15.772800	186.808959	16.450604	12.955346	3.704055
specularity	129.222652	43.072263	14.677605	74.712240	63.722877	16.649455	14.522926
Shape	195.110579	13.611480	13.378924	16.809748	27.200487	36.303328	12.708082
Motionc	73.601444	23.368815	13.177996	41.463503	41.078864	28.393178	13.227517
Confusion	7.912099	10.284466	5.964288	5.163981	13.702894	4.508166	4.834151
Low contrast	64.455336	45.932675	33.128893	30.408819	108.949187	25.565931	6.128211
Moving camera	225.216114	7.651350	32.740981	21.050286	12.944514	21.745703	11.347053
Zooming camera	13.935250	73.807708	11.885161	99.897294	41.697262	22.216277	6.164569
Clip730	8.068376	12.068048	17.595768	28.570511	41.438430	92.027791	5.471521
Clip152	100.761389	195.092011	168.013769	172.403973	41.188876	94.604120	38.154898
Clip187	25.809414	86.794811	157.218992	90.562039	102.678089	64.981330	4.845389
Clip284	30.290749	35.593709	34.037194	66.725242	65.170559	26.443014	12.219050
Clip442	85.235805	95.701956	50.343628	83.312501	75.672177	48.166680	7.877701
Clip498	33.489636	14.699226	10.673971	17.003137	20.333979	17.846120	5.516157
Clip233	12.524848	34.792787	25.246487	40.189297	40.455687	22.395450	8.110710
Clip790	49.445279	49.055761	29.931174	47.763538	204.462591	39.698874	12.262466
Clip796	2.579731	2.199148	4.968583	2.310338	65.141472	2.853344	2.719945
Clip249	29.794407	30.931084	26.985849	28.795526	6.698778	27.347306	4.967117
Trans	268.343388	39.333038	177.186029	42.258811	11.310398	168.902250	10.315606
Faceocc1	23.587613	78.167291	29.753680	12.474893	40.854845	11.930419	22.141050
Carscale	75.751940	24.529978	83.543614	33.052647	18.080219	76.641049	3.949226
Jogging	27.772805	98.316951	93.187874	98.407995	1.989573	90.302107	95.719804
Singer1	18.784432	3.442082	69.227230	2.956170	155.814957	13.301354	3.622780
Trellis	42.245188	7.536595	56.221727	6.294823	6.989458	17.342230	6.334139

Table 6 Center location error. Red: indicates best value, pink: indicates second best value and green: indicates third best.

of Fig. 16, Crossing sequence of Fig. 17, Low contrast and Light sequences of Fig. 18, Clip249, Clip284, Clip442, Clip730 sequences of Fig. 19. The target undergoes large scale change in these images due to object movement, whereas Singer1 of Fig. 16, Moving camera and Zooming camera of Fig. 18, the target changes its scale due to camera motion (or zooming). From these figures, it is shown that ASLA and SCM tried to adapt the scale but was unable to adapt actual scale of the object, whereas DFT, MTT, KCF techniques failed to adapt large scale change of the object. SPT provided better results than other existing techniques for sequences where objects underwent scale changes, but failed for large scale variation. On the other hand, as the proposed method extracts contour of the object, it is able to properly track the object with large scale variation.

In the Trans sequence of Fig.16, the Bmx, Iceskate and Octopus sequences of Fig.17, the objects change their appearances significantly with their scales. The Trellis sequence of Fig. 16 changes its pose under illumination variation condition. In Clip790 and Clip152 of Fig. 19, the objects change their pose in camouflaged environment. In these sequences, KCF and SPT tried to track the object properly, but due to scale change and occurrence of camouflage, after some frames, they fail to provide good results. However, the proposed method uses local information to detect the object, and thus pose change does not create a problem for the proposed method.

Shape deformation: The Trans sequence of Fig. 16, Octopus, Iceskate sequences of Fig.17 and Shape sequence of Fig. 17 show examples where drastic shape deformation occurs, tracking algorithms using holistic appearance models are unlikely to perform well (e.g., MTT and KCF). Other trackers such as ASLA, SCM, SPT also generate inaccurate results and their tracking windows cover a small portion of the object with a few number of successfully tracked frames. On the other hand, shape deformation can not create a problem for the proposed method for extracting contour of such objects. Hence, the proposed method can track shape deformable objects successfully.

Camouflaged object: The performances of the trackers are evaluated on sequences containing camouflaged objects. Clip187, Clip233, Clip498, Clip796 sequences of Fig. 19 have camouflaged objects with slow motion. From these figures, it is seen that all these trackers try to successfully track the camouflaged ob-

Sequences	DFT	ASLA	MTT	SCM	SPT	KCF	PM
bmx	0.198994	0.206489	0.141809	0.171547	0.230473	0.196422	0.928814
Butterfly	0.297064	0.006683	0.002663	0.019546	0.041330	0.409660	0.909362
Crossing	0.497065	0.094643	0.533404	0.328756	0.467039	0.493698	0.554065
Iceskate	0.346022	0.174792	0.062168	0.093337	0.091373	0.526962	0.568468
Octopus	0.286723	0.328906	0.205906	0.258324	0.108520	0.246128	0.861250
Sphere	0.372123	0.105290	0.056870	0.181065	0.512848	0.656769	0.683004
Light	0.036534	0.501686	0.685550	0.030745	0.666188	0.668888	0.880991
specularity	0.516896	0.670966	0.813402	0.606887	0.671278	0.700844	0.885334
Shape	0.257372	0.623641	0.788649	0.739798	0.563029	0.648203	0.837811
Motionc	0.455324	0.658334	0.686720	0.602468	0.541738	0.616924	0.872202
Confusion	0.859137	0.798740	0.875350	0.852384	0.780385	0.894058	0.870293
Low contrast	0.482756	0.570736	0.647150	0.678614	0.132290	0.651701	0.914405
Moving camera	0.012042	0.617392	0.461850	0.625365	0.763915	0.468915	0.619226
Zooming camera	0.536343	0.384562	0.573494	0.382404	0.515667	0.523091	0.860374
Clip730	0.289308	0.433153	0.505263	0.345981	0.297017	0.255194	0.851651
Clip152	0.135127	0.039828	0.052065	0.048638	0.281886	0.161266	0.558524
Clip187	0.467013	0.364163	0.141122	0.351481	0.337268	0.350641	0.936252
Clip284	0.674343	0.630456	0.670926	0.504710	0.385538	0.713322	0.855343
Clip442	0.311125	0.479023	0.514813	0.454602	0.346182	0.329878	0.903900
Clip498	0.617117	0.742313	0.765959	0.704595	0.537662	0.734047	0.863951
Clip233	0.775553	0.659731	0.715032	0.616157	0.602272	0.739076	0.905239
Clip790	0.505272	0.559807	0.548776	0.562473	0.108290	0.547848	0.859924
Clip796	0.939205	0.835671	0.908414	0.837906	0.487918	0.938508	0.891181
Clip249	0.505731	0.382954	0.547316	0.407107	0.529238	0.526891	0.854965
Trans	0.009384	0.546260	0.246554	0.528747	0.810588	0.092383	0.811549
Faceocc1	0.688809	0.298117	0.580104	0.749549	0.573050	0.795908	0.375153
Carscale	0.417602	0.551030	0.240763	0.433879	0.429623	0.418725	0.819184
Jogging	0.201439	0.160345	0.122781	0.150745	0.744170	0.184589	0.125540
Singer1	0.357793	0.437791	0.160772	0.496452	0.170572	0.361830	0.695146
Trellis	0.369432	0.664774	0.279005	0.752783	0.598859	0.489068	0.671104

Table 7 Average tracking accuracy. Red: indicates best value, pink: indicates second best value and green: indicates third best.

jects. However, MTT, ASLA, SCM perform better than KCF and SPT as local sparse representation is considered for appearance modeling. The proposed method provides the best result among them. In case of Clip152, Clip249, clip284, Clip442, Clip730 sequences of Fig. 19 which contain camouflaged object with scale variation and in Clip790 sequence of Fig. 19 containing camouflaged object which changes it appearance. All the existing trackers try to properly track the objects; but due to scale and appearance changes, after few frames they fail to track the object properly. On the other hand, the proposed method successfully tracks the object properly in such complex environment.

Occlusion: We evaluate the performance of tracking algorithms including the proposed technique on sequences where the objects undergo partial or heavy occlusions several times. In the Carscale sequence of Fig. 16, the object undergoes partial occlusion; whereas in Faceocc1 and Jogging sequences of Fig. 16, the object undergoes heavy occlusion. All existing trackers try to successfully track the occluded object. But due to fast motion and scale change, they fail to successfully track the objects after a few number of frames (e.g., Carscale#252 Jogging#307). Incase of partial occlusion, the proposed method successfully tracks the object. But for full occlusion, the proposed method fails to track the object due to loss of object information.

3.5 Execution Time Analysis

Sequences	DFT	ASLA	MTT	SCM	SPT	KCF	PM
200	0.1793	0.4450	1.0429	4.1442	2.5735	0.0051	0.5321

Table 8 Average execution time (seconds) for tracking object in a single frame. Red: indicates best value, pink: indicates second best, green: indicates third best.

Table 8 summaries the average execution time for tracking objects in a single frame using different techniques. From the table, it is seen that KCF is faster among all algorithms. Whereas SCM technique takes more time to track an object in a single frame. DFT and ASLA take less average execution time than the proposed method. On the other hand, the proposed method takes less execution time than MTT, SCM and

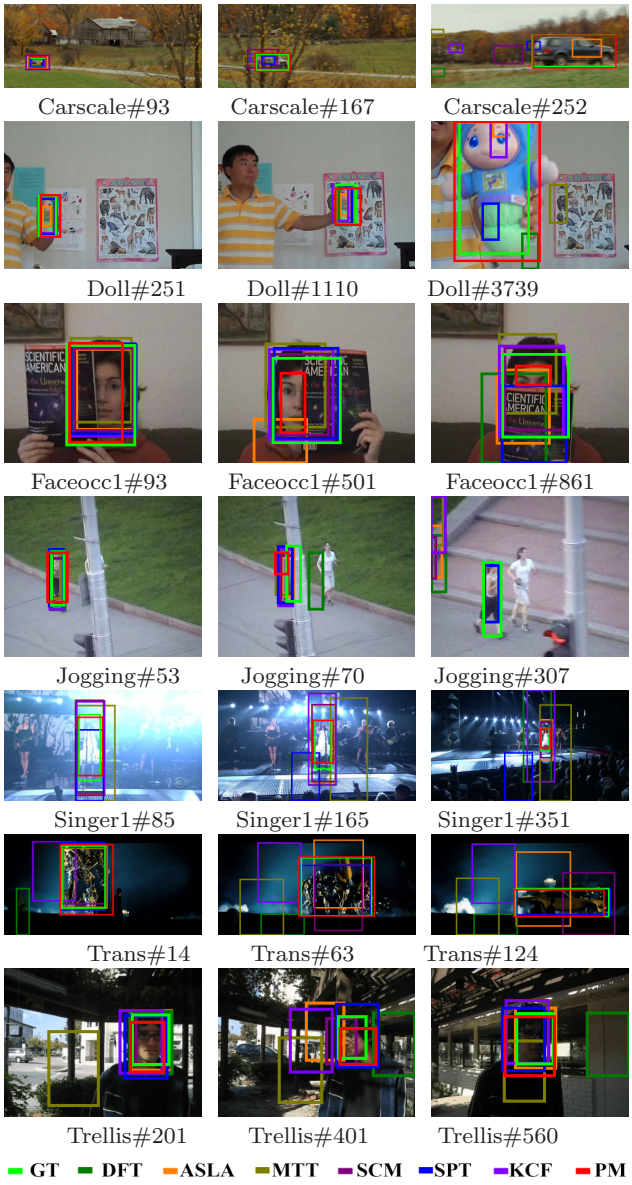

Fig. 16 Tracking results on Visual Tracker Benchmark sequences.

SPT. Therefore, the proposed method needs moderate amount of time to track the object in a single frame.

4 Discussion and Future Work

In this work it is established that the proposed integrated feature set from multi-cue is able to increase the separability between the camouflaged object and its surroundings. The proposed modified PNN requires small training samples rather than the whole training set and can better detect the camouflaged object efficiently. The proposed global and local fuzzy energy based active contour model uses the region information,

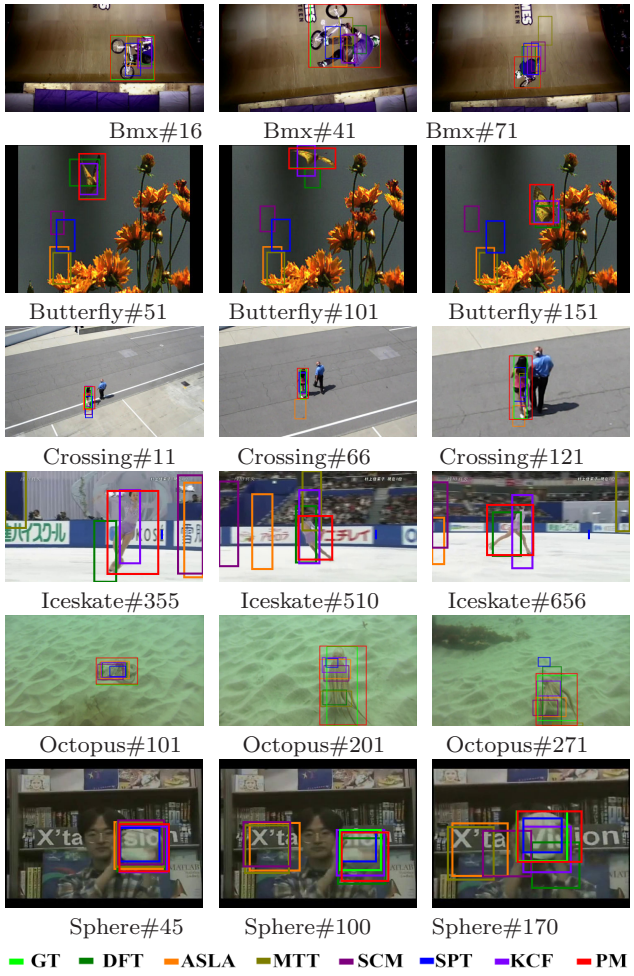

Fig. 17 Tracking results on VOT2015 Challenge sequences.

is able to extract the contour of the detected object and finally track the object properly.

4.1 Extension to Multiple Objects Tracking

Though the tracking results reported in this article highlight only a single object, it can also be extended to multiple objects tracking by considering multi-class (multiple objects and background) classification problem instead of two-class (object and background) classification [17]. After detecting objects using the modified PNN in the t^{th} frame, contours of the detected objects are extracted by the proposed fuzzy energy based active contour model and track the objects. Here, we assume that the sequence contains R numbers of different objects $l_{obj1}, l_{obj2}, . ., l_{objR}$ and a background l_{bg}. Initially objects are given by the user. Similar energy function given in Eq. (15) of each object is defined. By minimizing energy functions, contours of the objects are extracted and the objects are tracked. As an illustration,

Fig. 18 Tracking results on ALOV++ sequences.

some results of Clip796 sequence are given in Fig. 20. From this figure, it is seen that the proposed method provides acceptable results for tracking multiple objects. To measure the performance (quantitatively) of the proposed algorithm for multiple objects tracking, two values MOTA and MOTP are calculated. For this sequence, MOTA=1 & MOTP=0.8418 and these values indicate that the proposed method can provide acceptable results for multiple objects tracking also.

4.2 Effect of Smoothing Parameter σ

Accuracy of PNN depends on smoothing parameter σ [65]. In this work, σ is chosen experimentally. For different values of σ, different (object detection) results are obtained. Figs. 21 and 22 display camouflaged object detection results of Clip152 and Clip249 sequences, respectively, using the proposed modified PNN with different values of smoothing parameter σ. From these

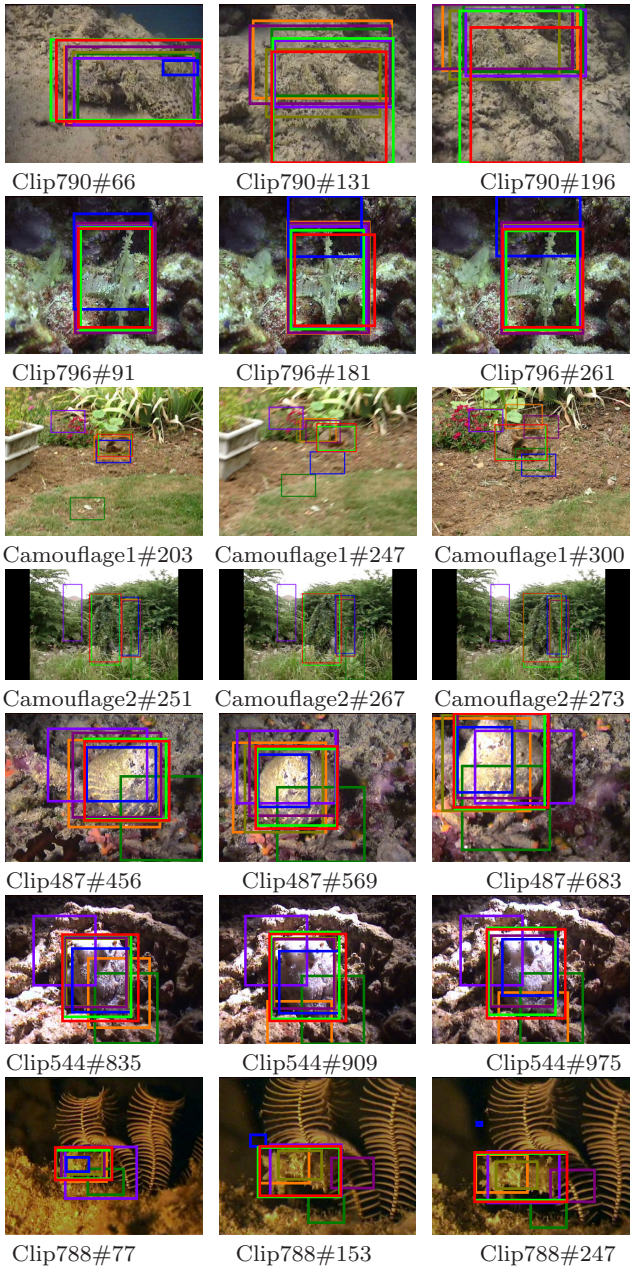

Fig. 19 Tracking results on Reef Video Clip sequences.

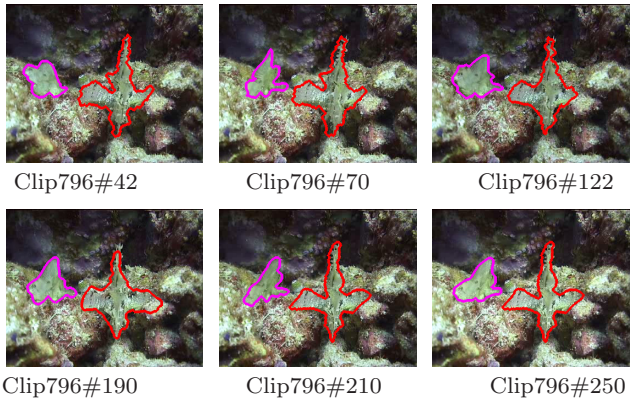

Fig. 20 Tracking results of multiple objects on Clip796 sequence.

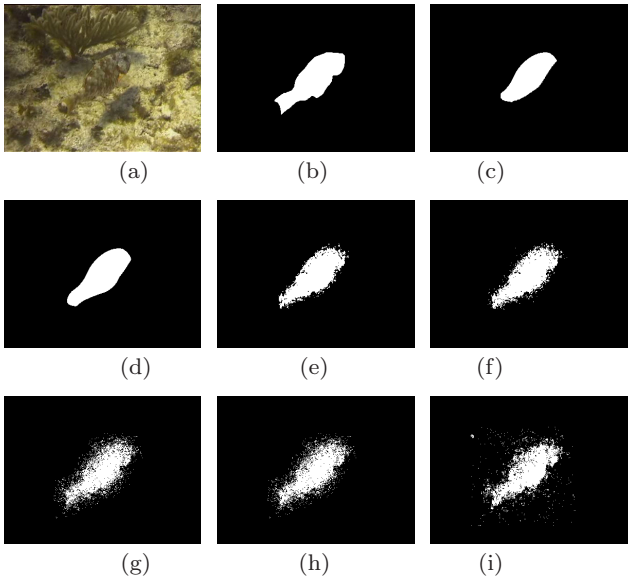

Fig. 21 (a) Original frame; (b) ground truth; object detection in Clip152 sequence using the modified PNN with (c) $\sigma = 100.0$; (d) $\sigma = 30.0$; (e) $\sigma = 5.0$; (f) $\sigma = 1.0$; (g) $\sigma = 0.5$; (h) $\sigma = 0.1$ and (i) $\sigma = 0.05$.

different values of σ							
Sequence	σ=100.0	σ=30.0	σ=5.0	σ=1.0	σ=0.5	σ=0.1	σ=0.05
*Clip*152	0.58592	0.6879	0.9886	0.9866	0.9753	0.9763	0.7845
*Clip*249	0.6928	0.7923	0.9953	0.9956	0.9926	0.9922	0.6907

Table 9 Object detection accuracy for different values of σ.

figures, it is observed that for large value of $\sigma > 5$ (Figs. 21(c), (d) and 22(c), (d)), objects are not detected properly. More parts of the object are detected as background. It is also observed that for small values of $\sigma < 0.1$ (Figs. 21(i) and 22(i)), objects are detected along with more background pixels. For other values of $\sigma \in [0.1,\ 5.0]$, similar kinds of results are obtained (Figs. 21(e), (f), (g), (h) and 22(e), (f), (g), (h)). Table 9 shows the detection accuracy of the proposed method for different values of σ. This table also highlights the effect of parameter σ for object detection.

4.3 Effect of Parameter β

In this section, the role of parameter β for controlling the weights of global and local energies (or forces or information or terms) of the proposed fuzzy energy function is discussed. Here, β is $0 \leq \beta \leq 1$. If a lower value of β is chosen, the global term contributes less than the local term in the proposed fuzzy energy function. On the other hand, higher value of β indicates that the global term may prevent the local force for extracting

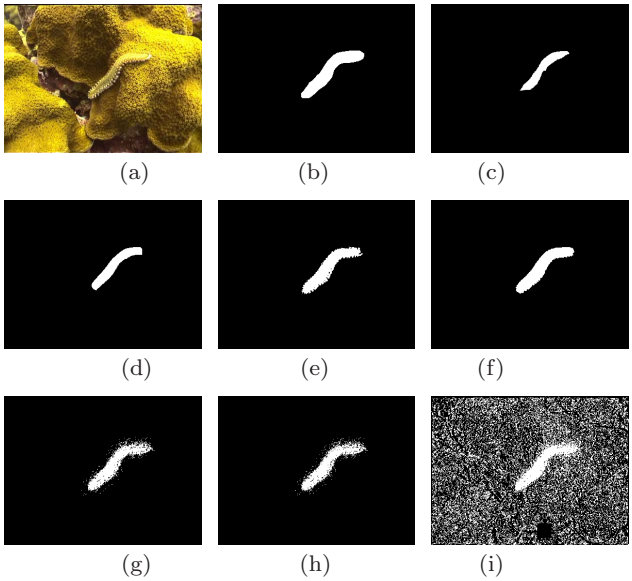

Fig. 22 (a) Original frame; (b) ground truth; object detection in Clip249 sequence using the modified PNN with (c) $\sigma = 100.0$; (d) $\sigma = 30.0$; (e) $\sigma = 5.0$; (f) $\sigma = 1.0$; (g) $\sigma = 0.5$; (h) $\sigma = 0.1$ and (i) $\sigma = 0.05$.

exact boundary of the object in the t^{th} frame. Moderate value of β (= 0.5) indicates that the global and local terms have equal contribution in the proposed fuzzy energy function.

To visually illustrate the effect of parameter β, tracking results of Clip249 sequence for different values of β are given in Fig. 23. From this figure (Fig. 23(d)), it is seen that tracking result is not proper due to more contribution of the global term than the local term and is unable to extract the boundary of the objects. Figs. 23(f), (h) and (j) highlight that similar tracking results are obtained with different values of β=0.7, 0.5, 0.1, 0.01. Detection accuracy and tracking accuracy for different values of parameter β are summarized in Tables 10 and 11, respectively. Table 10 highlights that similar object detection result is obtained by varying the value of parameter β as it does not have any role for detection whereas Table 11 indicates that different tracking results are obtained by varying values of β. However, in this work we chose $\beta = 0.5$ for all experiments.

different values of β					
Sequence	β=0.9	β=0.7	β=0.5	β=0.1	β=0.01
*Clip*249	0.9926	0.9926	0.9926	0.9926	0.9926

Table 10 Object detection accuracy for different values of β.

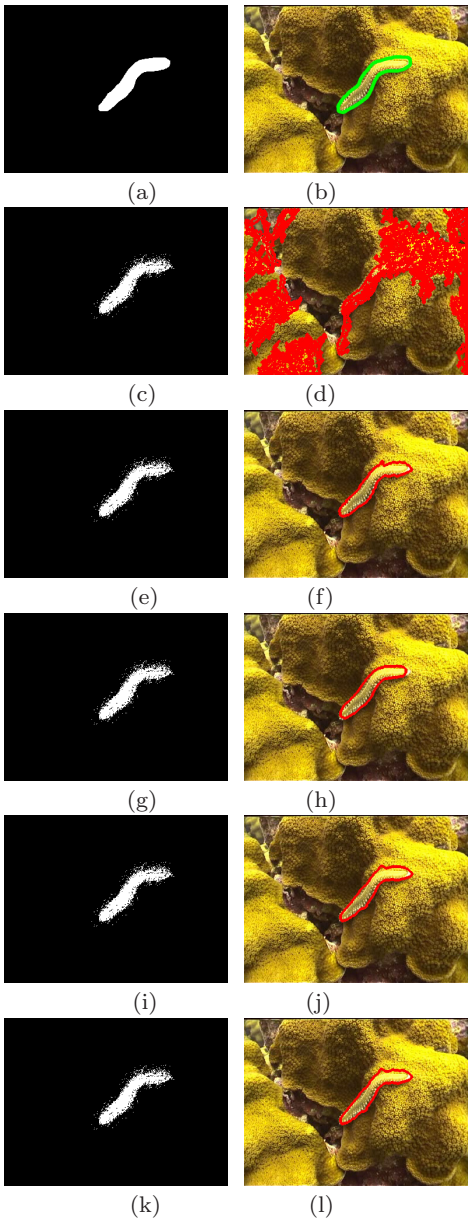

Fig. 23 (a) & (b) Ground truth object detection and tracker; Results of camouflaged object detection and tracking in Clip249 sequence using the modified PNN and the proposed fuzzy active contour with (c) & (d) $\sigma = 0.1$, $\lambda_1 = \lambda_2 = 1$, $\beta = 0.9$; (e) & (f) $\sigma = 0.1$, $\lambda_1 = \lambda_2 = 1$, $\beta = 0.7$; (g) & (h) $\sigma = 0.1$, $\lambda_1 = \lambda_2 = 1$, $\beta = 0.5$; (i) & (j) $\sigma = 0.1$, $\lambda_1 = \lambda_2 = 1$, $\beta = 0.1$; (k) & (l) $\sigma = 0.1$, $\lambda_1 = \lambda_2 = 1$, $\beta = 0.01$.

4.4 Effect of Parameters λ_1 and λ_2

Two parameters λ_1 and λ_2 in the proposed energy function (given in Eq. (15)) are the weights of integrals over regions Ω_1 (i.e., inside(C)) and Ω_2 (i.e., outside(C)) of the contour C. For all experiments, we consider λ_1=λ_2 to balance the impotence of each side during the minimization of the proposed energy function given in Eq.(15). If we consider λ_1 to be greater than λ_2, then the region

different values of β					
Sequence	β=0.9	β=0.7	β=0.5	β=0.1	β=0.01
*Clip*249	0.0719	0.8375	0.8352	0.8355	0.8314

Table 11 Tracking accuracy for different values of β.

inside the contour i.e., Ω_1 is given more importance than the outside region of the contour i.e., Ω_2 and vice versa. Fig. 24 displays the tracking results for different values of λ_1 and λ_2. From these figures, it is observed that when $\lambda_1 > \lambda_2$, contour is moved towards the inner region of the target (see Fig. 24(d)). When $\lambda_1 < \lambda_2$, contour is moved away from the exact object boundary. For visual illustration, see Figs. 24(f), (h) and (j). On the other hand, for $\lambda_1 = \lambda_2$, the exact contour of the object is obtained. Fig. 24(l) displays the tracking result when $\lambda_1 = \lambda_2$. Tables 12 and 13 summarize the detection accuracy and tracking accuracy for different values of λ_1 and λ_2, respectively. Table 12 highlights that for different values of λ_1 and λ_2, similar object detection results are obtained. Whereas Table 13 highlights that the best tracking result is obtained when λ_1=λ_2. In our work, $\lambda_1 = \lambda_2 = 1$ is considered for all experiments.

different values of λ_1 and λ_2					
Sequence	L_1	L_2	L_3	L_4	L_5
*Clip*249	0.9926	0.9926	0.9926	0.9926	0.9926

Table 12 Object detection accuracy based on L_1: λ_1=1.1 & λ_2=1.0; L_2: λ_1=1.0 & λ_2=1.1; L_3: λ_1=1.0 & λ_2=1.3; L_4: λ_1=1.0 & λ_2=1.5 and L_5: λ_1=1.0 & λ_2 =1.0.

different values of λ_1 and λ_2					
Sequence	L_1	L_2	L_3	L_4	L_5
*Clip*249	0.7879	0.6938	0.6059	0.6912	0.8532

Table 13 Tracking accuracy based on L_1: λ_1=1.1 & λ_2=1.0; L_2: λ_1=1.0 & λ_2=1.1; L_3: λ_1=1.0 & λ_2=1.3; L_4: λ_1=1.0 & λ_2=1.5 and L_5: λ_1=1.0 & λ_2 =1.0; red: indicates best result.

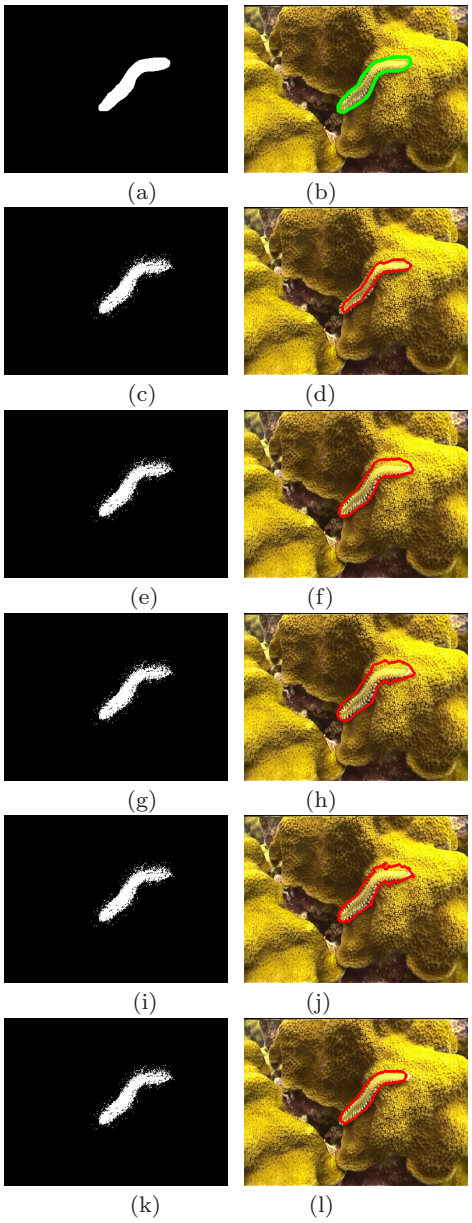

Fig. 24 (a) & (b) Ground truth object detection and tracker; camouflaged object detection and tracking in Clip249 sequence using the modified PNN and the proposed fuzzy active contour with (c) & (d) $\sigma = 0.1$, $\lambda_1 = 1.1$, $\lambda_2 = 1$, $\beta = 0.5$; (e) & (f) $\sigma = 0.1$, $\lambda_1 = 1$, $\lambda_2 = 1.1$, $\beta = 0.5$; (g) & (h) $\sigma = 0.1$, $\lambda_1 = 1$, $\lambda_2 = 1.3$, $\beta = 0.5$; (i) & (j) $\sigma = 0.1$, $\lambda_1 = 1$, $\lambda_2 = 1.5$, $\beta = 0.5$; (k) & (l) $\sigma = 0.1$, $\lambda_1 = \lambda_2 = 1$, $\beta = 0.5$

4.5 Occlusion Handling

Several factors affect the performance of tracking algorithm. Occlusion is one of such factor. Two types of occlusion may occur: i) occlusions between two or more objects of interests; ii) occlusions between an object of interest and an object of the background. Both of them may be either partial or full. Here, behavior of the proposed algorithm for handling last problem is discussed. In the proposed method, modified PNN (pixel based classification technique) detects the target and fuzzy active contour extracts the contour of the target. The proposed method can track objects with partial occlusion (less than 20%). Fig. 25(a) shows the performance of the proposed algorithm for tracking (less than 20%) occluded object. For partial occlusion (more than 20%) and full occlusion, the proposed technique fails to track the object due to inaccurate detection results and loss of object information. Figs. 25(b) and (c) show the poor performance of the proposed technique for tracking occluded (more than 20% for partial and

full) objects. Table 14 shows the quantitative measures for performance of the proposed method for occluded object tracking. Similar observation is found from this table.

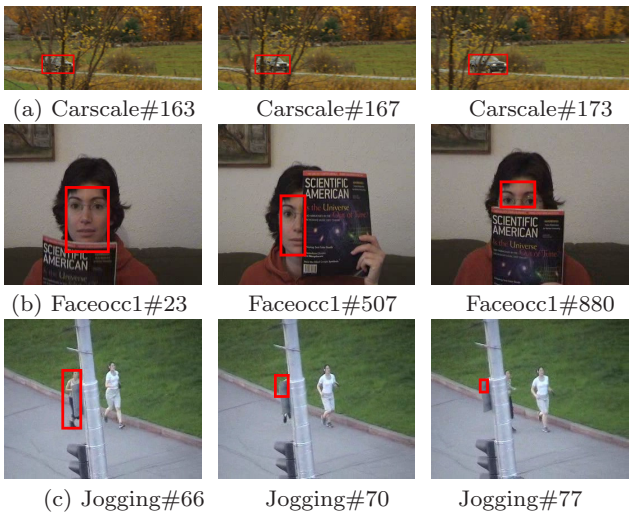

(a) Carscale#163 Carscale#167 Carscale#173

(b) Faceocc1#23 Faceocc1#507 Faceocc1#880

(c) Jogging#66 Jogging#70 Jogging#77

Fig. 25 Performance of the proposed algorithm for tracking occluded object.

Sequence	average center location	average tracking accuracy
carscale	3.9492	0.8192
faceocc1	22.1411	0.3752
jogging	15.7198	0.3955

Table 14 Tracking accuracy of the occluded object using the proposed method.

4.6 Future Work

The proposed technique considers only three features for integrating. In future, motion information may be taken into account to generate more features. In this work, all features are given equal weights during integration. Weights based on importance of each feature may be provided during integration in future. We will also consider some other color spaces other than CIElab (developed based on human eye or biological vision system) in future.

Though, in this work σ is chosen experimentally, in literature, several techniques [39,49,83] are proposed to select proper value of σ. σ may be selected automatically by developing some optimization technique.

The proposed method does not explicitly consider occlusion problem. Attention may be given to develop, some objective functions based on object detection results (obtained by the modified PNN) to detect occurrence of occlusion automatically. Due to occlusion, object information is not available in that frame. So prior information i.e., shape of object (from previous frame) may be considered as object information in the frame where occlusion occurred. To estimate the location of the target, particle filter can be considered. Therefore, use of shape prior and particle filter with the proposed method may help handle occlusion problem in a better way.

5 Conclusions

In this article, a tracking-by-detection algorithm is proposed to detect and track camouflaged objects. We propose to represent an object in terms of feature vectors of color, shape and texture which increases the separability between the camouflaged object and background. Object is detected by the modified probabilistic neural network and finally tracking is done by devising fuzzy energy based active contour model. The proposed technique is able to track objects under camouflaged as well as several other (illumination variation, scale change, rotation, pose change) complex environments. Experimental results and analysis demonstrate that the proposed method outperforms state-of-the-art techniques of object detection for various complex (including camouflaged) environments.

Acknowledgements

The authors like to thank the editor and the reviewers for their thorough and constructive comments, which helped a lot to enhance the quality of the manuscript. Funding by U. S. Army through the project “Processing and Analysis of Aircraft Images with Machine Learning Techniques for Locating Objects of Interest” (Contract No. FA5209-08-P-0241) is also gratefully acknowledged.

References

1. Akhloufi, M.A., Bendada, A.: Locally adaptive texture features for multispectral face recognition. In: IEEE International Conference on Systems Man and Cybernetics (SMC), pp. 3308–3314 (2010)
2. Avidan, S.: Ensemble tracking. IEEE Transactions on Pattern Analysis and Machine Intelligence **29**(2), 261–271 (2007)
3. Babenko, B., Yang, M., Belongie, S.: Robust object tracking with online multiple instance learning. IEEE Transactions on Pattern Analysis and Machine Intelligence **33**(8), 1619–1632 (2011)
4. Bandouch, J., Jenkins, O.C., Beetz, M.: A self-training approach for visual tracking and recognition of complex human activity patterns. International Journal of Computer Vision **99**(2), 166–189 (2012)

5. Bishop, C.M.: Neural Networks for Pattern Recognition. Oxford, Clarendon Press, (1995)
6. Boult, T.E., Micheals, R.J., Gao, X., Eckmann, M.: Into the woods: Visual surveillance of noncooperative and camouflaged targets in complex outdoor settings. Proceedings of the IEEE **89**(10), 1382–1402 (2001)
7. Burrascano, P.: Learning vector quantization for the probabilistic neural network. IEEE transactions on Neural Networks **2**(4), 458–461 (1990)
8. Caselles, V., Kimmel, R., Sapiro, G.: Geodesic active contours. International journal of Computer Vision **22**(1), 61–79 (1997)
9. Challa, S., Morelande, M.R., Musicki, D., Evans, R.J.: Fundamentals of Object Tracking. Cambridge, U. K: Cambridge University Press (2011)
10. Chan, T.F., Vese, L.A.: Active contours without edges. IEEE Transactions on Image Processing **10**(2), 266–277 (2001)
11. Chandesa, T., Pridmore, T., Bargiela, A.: Detecting occlusion and camouflage during visual tracking. In: IEEE International Conference on Signal and Image Processing Applications (ICSIPA), pp. 468–473 (2009)
12. Cohen, L.D., Kimmel, R.: Global minimum for active contour models: A minimal path approach. International Journal of Computer Vision **24**(1), 57–78 (1997)
13. Conte, D., Foggia, P., Percannella, G., Tufano, F., Vento, M.: An algorithm for detection of partially camouflaged people. In: 6th IEEE International Conference on Advanced Video and Signal Based Surveillance (AVSS), pp. 340–345 (2009)
14. Copeland, A.C., Trivedi, M.M.: Models and metrics for signature strength evaluation of camouflaged targets. In: AeroSense, pp. 194–199 (1997)
15. Cremers, D., Rousson, M., Deriche, R.: A review of statistical approaches to level set segmentation: Integrating color, texture, motion and shape. International Journal of Computer Vision **72**(2), 195–215 (2007)
16. Dalal, N., Triggs, B.: Histograms of oriented gradients for human detection. In: Proceedings of IEEE Conference on Computer Vision and Pattern Recognition, vol. 1, pp. 886–893 (2005)
17. Desai, C., Ramanan, D., Fowlkes, C.C.: Discriminative models for multi-class object layout. International Journal of Computer Vision **95**(1), 1–12 (2011)
18. Di Lascio, R., Foggia, P., Percannella, G., Saggese, A., Vento, M.: A real time algorithm for people tracking using contextual reasoning. Computer Vision and Image Understanding **117**(8), 892–908 (2013)
19. Du, H., Jin, X., Mao, X.: Digital camouflage images using two-scale decomposition. In: Computer Graphics Forum, pp. 2203–2212 (2012)
20. Fox, C.W.: An Introduction to the Calculus of Variations. New York, Dover Publications Inc. (1988)
21. Freeman, W.T., Roth, M.: Orientation histograms for hand gesture recognition. In: IEEE International Workshop on Automatic Face and Gesture Recognition, pp. 296–301 (1995)
22. Gonzalez, R.F., Woods, R.E.: Digital Image Processing. Singapore: Pearson Education (2008)
23. Gretzmacher, F.M., Ruppert, G.S., Nyberg, S.: Camouflage assessment considering human perception data. In: Aerospace/Defense Sensing and Controls, pp. 58–67 (1998)
24. Hao, W., Zhang, B., Tian, W.: Head tracking by means of probabilistic neural networks. Measurement Science and Technology **18**(7), 1999–2009 (2007)
25. Haralick, R.M., Shanmugam, K., Dinstein, I.H.: Textural features for image classification. IEEE Transactions on Systems, Man and Cybernetics **3**(6), 610–621 (1973)
26. Hare, S., Saffari, A., Torr, P.H.: Struck: Structured output tracking with kernels. In: IEEE International Conference on Computer Vision (ICCV), pp. 263–270 (2011)
27. Harville, M., Gordon, G., Woodfill, J.: Foreground segmentation using adaptive mixture models in color and depth. In: Proceedings on IEEE Workshop on Detection and Recognition of Events in Video, pp. 3–11 (2001)
28. He, L., Osher, S.: Solving the Chan-Vese model by a multiphase level set algorithm based on the topological derivative. In: Proceedings of the 1st International Conference on Scale Space and Variational Methods in Computer Vision, SSVM, pp. 777–788 (2007)
29. Henriques, J.F., Caseiro, R., Martins, P., Batista, J.: High-speed tracking with kernelized correlation filters. IEEE Transactions on Pattern Analysis and Machine Intelligence **37**(3), 583–596 (2015)
30. Hou, J.Y.Y.H.W., Li, J.: Detection of the mobile object with camouflage color under dynamic background based on optical flow. Procedia Engineering **15**, 2201–2205 (2011)
31. Huang, Z.Q., Jiang, Z.: Tracking camouflaged objects with weighted region consolidation. In: Proceedings on Digital Image Computing: Techniques and Applications (DICTA), pp. 24–31 (2005)
32. Jia, X., Lu, H., Yang, M.H.: Visual tracking via adaptive structural local sparse appearance model. In: IEEE Conference on Computer Vision and Pattern Recognition (CVPR), pp. 1822–1829 (2012)
33. KaewTrakulPong, P., Bowden, R.: A real time adaptive visual surveillance system for tracking low-resolution colour targets in dynamically changing scenes. Image and Vision Computing **21**(10), 913–929 (2003)
34. Kalal, Z., Mikolajczyk, K., Matas, J.: Tracking-learning-detection. IEEE Transactions on Pattern Analysis and Machine Intelligence **34**(7), 1409–1422 (2012)
35. Kass, M., Witkin, A., Terzopoulos, D.: Snakes: Active contour models. International Journal of Computer Vision **1**(4), 321–331 (1988)
36. Kasturi, R., Goldgof, D., Soundararajan, P., Manohar, V., Garofolo, J., Bowers, R., Boonstra, M., Korzhova, V., Zhang, J.: Framework for performance evaluation of face, text, and vehicle detection and tracking in video: Data, metrics and protocol. IEEE Transactions on Pattern Analysis and Machine Intelligence **31**(2), 319–336 (2009)
37. Krinidis, S., Chatzis, V.: Fuzzy energy-based active contours. IEEE Transactons on Image Processing **18**(12), 2747–2755 (2009)
38. Krinidis, S., Krinidis, M.: Fuzzy energy-based active contours exploiting local information. In: 8th International Conference on Artificial Intelligence Applications and Innovations (AIAI'12), pp. 27–30 (2012)
39. Kusy, M., Kluska, J.: Probabilistic neural network structure reduction for medical data classification. In: Artificial Intelligence and Soft Computing, pp. 118–129 (2013)
40. Kwon, J., Lee, K.M.: Visual tracking decomposition. In: Proceedings of IEEE Conference on Computer Vision and Pattern Recognition (CVPR), pp. 1269–1276 (2010)
41. Lan, X., Ma, A.J., Yuen, P.C.: Multi-cue visual tracking using robust feature-level fusion based on joint sparse representation. In: IEEE Conference on Computer Vision and Pattern Recognition (CVPR), pp. 1194–1201 (2014)
42. Lankton, S., Tannenbaum, A.: Localizing region-based active contours. IEEE Transactions on Image Processing **17**(11), 2029–2039 (2008)

43. Levi, K., Weiss, Y.: Learning object detection from a small number of examples: the importance of good features. In: Proceedings of IEEE Conference on Computer Vision and Pattern Recognition, vol. 2, pp. 53–60 (2004)
44. Li, C., Kao, C.Y., Gore, J.C., Ding, Z.: Minimization of region-scalable fitting energy for image segmentation. IEEE Transactions on Image Processing **17**(10), 1940–1949 (2008)
45. Li, C., Xu, C., Gui, C., Fox, M.D.: Distance regularized level set evolution and its application to image segmentation. IEEE Transactions on Image Processing **19**(12), 3243–3254 (2010)
46. Li, X., Hu, W., Shen, C., Zhang, Z., Dick, A., Hengel, A.V.D.: A survey of appearance models in visual object tracking. ACM Transactions on Intelligent Systems and Technology **4**(4), 1–58 (2013)
47. Maggio, E., Cavallaro, A.: Video Tracking: Theory and Practice. West Sussex, U. K: John Wiley and Sons, Ltd. (2011)
48. Malathi, T., Bhuyan, K.M.: Foreground object detection under camouflage using multiple camera-based codebooks. In: Annual IEEE India Conference (INDICON), pp. 1–6 (2013)
49. Mao, K.Z., Tan, K.C., Ser, W.: Probabilistic neural-network structure determination for pattern classification. IEEE Transactions on Neural Networks **11**(4), 1009–1016 (2000)
50. Metz, C.E.: Basic principles of ROC analysis. In: Seminars in Nuclear Medicine, vol. 8, pp. 283–298. Elsevier (1978)
51. Mondal, A., Ghosh, S., Ghosh, A.: Efficient silhouette-based contour tracking using local information. Soft Computing pp. 1–21 (2014)
52. Mumford, D., Shah, J.: Optimal approximations by piecewise smooth functions and associated variational problems. Communications on Pure and Applied Mathematics **42**(5), 577–685 (1989)
53. Musavi, M.T., Chan, K.H., Hummels, D.M., Kalantri, K.: On the generalization ability of neural network classifiers. IEEE Transactions on Pattern Analysis and Machine Intelligence **16**(6), 659–663 (1994)
54. Ning, J., Zhang, L., Zhang, D., Wu, C.: Robust object tracking using joint color-texture histogram. International Journal of Pattern Recognition and Artificial Intelligence **23**(07), 1245–1263 (2009)
55. Ojala, T., Pietikäinen, M., Harwood, D.: A comparative study of texture measures with classification based on featured distributions. Pattern Recognition **29**(1), 51–59 (1996)
56. Osher, S., Sethian, J.A.: Fronts propagating with curvature dependent speed: algorithms based on hamilton-jacobi formulation. Journal of Computational Physics **79**(1), 12–49 (1988)
57. Pan, Y., Birdwell, D.J., Djouadi, S.M.: Efficient implementation of the Chan-Vese models without solving PDEs. In: Proceedings of International Workshop on Multimedia Signal Processing, pp. 350–353 (2006)
58. Raghu, P., Yegnanarayana, B.: Supervised texture classification using a probabilistic neural network and constraint satisfaction model. IEEE Transactions on Neural Networks **9**(3), 516–522 (1998)
59. Ross, D.A., Lim, J., Lin, R.S., Yang, M.H.: Incremental learning for robust visual tracking. International Journal of Computer Vision **77**(1-3), 125–141 (2008)
60. Santner, J., Leistner, C., Saffari, A., Pock, T., Bischof, H.: PROST: Parallel robust online simple tracking. In: Proceedings of IEEE Conference on Computer Vision and Pattern Recognition (CVPR), pp. 723–730 (2010)
61. Sevilla-Lara, L., Learned-Miller, E.: Distribution fields for tracking. In: IEEE Conference on Computer Vision and Pattern Recognition (CVPR), pp. 1910–1917 (2012)
62. Shyu, K.K., Pham, V.T., Tran, T.T., Lee, P.L.: Global and local fuzzy energy-based active contours for image segmentation. Nonlinear Dynamics **67**(2), 1559–1578 (2012)
63. Singh, S.K., Dhawale, C.A., Misra, S.: Survey of object detection methods in camouflaged image. IERI Procedia **4**, 351–357 (2013)
64. Song, B., Chan, T.: A fast algorithm for level set based optimization. CAM-UCLA **68**, 02–68 (2002)
65. Specht, D.F.: Probabilistic neural networks. Neural networks **3**(1), 109–118 (1990)
66. Suard, F., Rakotomamonjy, A., Bensrhair, A.: Pedestrian detection using Infrared images and histograms of oriented gradients. In: IEEE Conference on Intelligent Vehicles, pp. 206–212 (2006)
67. Talu, M.F.: ORACM: Online region-based active contour model. Expert Systems with Applications **40**(16), 6233–6240 (2013)
68. Tan, X., Triggs, B.: Enhanced local texture feature sets for face recognition under difficult lighting conditions. IEEE Transactions on Image Processing **19**(6), 1635–1650 (2010)
69. Tang, S., Andriluka, M., Schiele, B.: Detection and tracking of occluded people. International Journal of Computer Vision **110**(1), 58–69 (2014)
70. Tran, T.T., Pham, V.T., Shyu, K.K.: Image segmentation using fuzzy energy-based active contour with shape prior. Journal of Visual Communication and Image Representation **25**(7), 1732–1745 (2014)
71. Traven, H.G.: A neural network approach to statistical pattern classification by semiparametric' estimation of probability density functions. IEEE Transactions on Neural Networks **2**(3), 366–377 (1991)
72. Wang, J., Yagi, Y.: Integrating color and shape-texture features for adaptive real-time object tracking. IEEE Transactions on Image Processing **17**(2), 235–240 (2008)
73. Wu, Y., Lim, J., Yang, M.H.: Online object tracking: A benchmark. In: IEEE Conference on Computer Vision and Pattern Recognition (CVPR), pp. 2411–2418 (2013)
74. Wu, Y., Ma, W., Gong, M., Li, H., Jiao, L.: Novel fuzzy active contour model with kernel metric for image segmentation. Applied Soft Computing **34**(2015), 301–311 (2015)
75. Yan, W., Weber, C., Wermter, S.: A hybrid probabilistic neural model for person tracking based on a ceiling-mounted camera. Journal of Ambient Intelligence and Smart Environments **3**(3), 237–252 (2011)
76. Yang, B., Nevatia, R.: Multi-target tracking by online learning a CRF model of appearance and motion patterns. International Journal of Computer Vision **107**(2), 203–217 (2014)
77. Yang, F., Lu, H., Yang, M.H.: Robust superpixel tracking. IEEE Transactions on Image Processing **23**(4), 1639–1651 (2014)
78. Yezzi, A., Kichenassamy, S., Kumar, A., Olver, P., Tannenbaum, A.: A geometric Snake model for segmentation of medical imagery. IEEE Transactions on Medical Imaging **16**(2), 199–209 (1997)
79. Yilmaz, A., Javed, O., Shah, M.: Object tracking: a survey. ACM Computing Surveys **38**(4), 1264–1291 (2006)
80. Zhang, K., Zhang, L., Song, H., Zhou, W.: Active contours with selective local or global segmentation: a new

formulation and level set method. Image and Vision Computing **28**(4), 668–676 (2010)
81. Zhang, T., Ghanem, B., Liu, S., Ahuja, N.: Robust visual tracking via structured multi-task sparse learning. International Journal of Computer Vision **101**(2), 367–383 (2013)
82. Zhang, X., Hu, W., Xie, N., Bao, H., Maybank, S.: A robust tracking system for low frame rate video. International Journal of Computer Vision pp. 1–26 (2015)
83. Zhong, M., Coggeshall, D., Ghaneie, E., Pope, T., Rivera, M., Georgiopoulos, M., Anagnostopoulos, G.C., Mollaghasemi, M., Richie, S.: Gap-based estimation: Choosing the smoothing parameters for probabilistic and general regression neural networks. Neural Computation **19**(10), 2840–2864 (2007)
84. Zhong, W., Lu, H., Yang, M.H.: Robust object tracking via sparse collaborative appearance model. IEEE Transactions on Image Processing **23**(5), 2356–2368 (2014)

A :Appendix

The proposed energy function F in Eq. (15) is convex with respect to u.

Proof

Let

$$F_A(\mathbf{X}^t) = \int_{\Omega} [u(\mathbf{X}^t)]^m \left\|I(\mathbf{X}^t) - C_1\right\|^2 d\mathbf{X}^t,\ \mathbf{X}^t \in \Omega \equiv \Re^2 \quad \text{(A.1)}$$

and

$$f_A(\mathbf{X}^t) = [u(\mathbf{X}^t)]^m \left\|I(\mathbf{X}^t) - C_1\right\|^2, \quad \text{(A.2)}$$

where $f_A : \Omega \to \Re$. Therefore, $F_A(\mathbf{X}^t) = \int_{\Omega} f_A(\mathbf{X}^t) d\mathbf{X}^t$.

Now let $\mathbf{X}_1 \equiv (x_1, y_1)$ and $\mathbf{X}_2 \equiv (x_2, y_2) \in \Omega$. For any $\theta \in [0, 1]$, we have

$$\begin{aligned}&\theta\mathbf{X}_1 + (1-\theta)\mathbf{X}_2\\ &= \theta\,(x_1, y_1) + (1-\theta)\,(x_2, y_2)\\ &= (\theta x_1 + (1-\theta)x_2, \theta y_1 + (1-\theta)y_2)\\ &= (\theta\,(x_1 - x_2) + x_2, \theta\,(y_1 - y_2) + y_2) \in \Omega \equiv \Re^2.\end{aligned}$$

Since $\theta\,(x_1 - x_2) + x_2 \in \Re$ as $x_1,\ x_2 \in \Re$ and $\theta \in [0, 1]$; and $\theta\,(y_1 - y_2) + y_2 \in \Re$ as $y_1,\ y_2 \in \Re$ and $\theta \in [0, 1]$. Therefore, the domain of f_A i.e., $\Omega \equiv \Re^2$ is convex.

Differentiating Eq. (A.2) w. r. t. u, we have

$$\frac{\partial f_A}{\partial u} = m\,[u(\mathbf{X}^t)]^{m-1} \left\|I(\mathbf{X}^t) - c_1\right\|^2.$$

Again differentiating $\frac{\partial f_A}{\partial u}$ w. r. t. u, we have

$$\frac{\partial^2 f_A}{\partial u^2} = m(m-1)\,[u(\mathbf{X}^t)]^{m-2} \left\|I(\mathbf{X}^t) - c_1\right\|^2.$$

Now $\frac{\partial^2 f_A}{\partial u^2} \geq 0$, since $m > 1$, $u(\mathbf{X}^t) \in [0, 1]$ and $\left\|I(\mathbf{X}^t) - c_1\right\|^2 \geq 0$.
Since domain of f_A is convex and $\frac{\partial^2 f_A}{\partial u^2} \geq 0$, therefore f_A is convex. Thus, $\forall \mathbf{Y}_1, \mathbf{Y}_2 \in \Omega \equiv \Re^2$ and $\theta \in [0, 1]$. The following relation

$$f_A(\theta\mathbf{X}_1 + (1-\theta_2)\mathbf{X}_2) \leq \theta f_A(\mathbf{X}_1) + (1-\theta) f_A(\mathbf{X}_2) \quad \text{(A.3)}$$

holds. Integrating both the sides of Eq.(A.3), we have

$$\begin{aligned}&\int_{\Omega} f_A(\theta\mathbf{X}_1 + (1-\theta)\mathbf{X}_2) d\mathbf{X}^t\\ &\leq \theta_2 \int_{\Omega} f_A(\mathbf{X}_1) d\mathbf{X}^t + (1-\theta) \int_{\Omega} f_A(\mathbf{X}_2) d\mathbf{X}^t.\end{aligned} \quad \text{(A.4)}$$

But $\int_{\Omega} f_A(\mathbf{X}^t) d\mathbf{X}^t = F_A(\mathbf{X}^t)$. Therefore, we have

$$F_A\left(\theta\mathbf{X}_1 + (1-\theta)\mathbf{X}_2\right) \leq \theta_2 F_A(\mathbf{X}_1) + (1-\theta) F_A(\mathbf{X}_2).$$

Hence, F_A is convex.

Similarly, let

$$F_B(\mathbf{X}^t) = \int_{\Omega} [1 - u(\mathbf{X}^t)]^m \left\|I(\mathbf{X}^t) - c_2\right\|^2 d\mathbf{X}^t, \quad \text{(A.5)}$$

and

$$f_B(\mathbf{X}^t) = [1 - u(\mathbf{X}^t)]^m \left\|I(\mathbf{X}^t) - c_2\right\|^2, \quad \text{(A.6)}$$

where $f_B : \Omega \to \Re$. Therefore $F_B(\mathbf{X}^t) = \int_{\Omega} f_B(\mathbf{X}^t) d\mathbf{X}^t$. In a similar way, we can prove that F_B is also convex.

Again let

$$F_{C_1}(\mathbf{Y}^t) = \int_{\Omega} W_{\mathbf{X}^t\mathbf{Y}^t} [1 - u(\mathbf{Y}^t)]^m \left\|I(\mathbf{Y}^t) - c_1\right\|^2 d\mathbf{Y}^t, \quad \text{(A.7)}$$

$$F_C(\mathbf{X}^t) = \int_{\Omega} [u(\mathbf{X}^t)]^m F_{C_1}(\mathbf{Y}^t) d\mathbf{X}^t, \quad \text{(A.8)}$$

$$f_{C_1}(\mathbf{Y}^t) = W_{\mathbf{X}^t\mathbf{Y}^t} [1 - u\,(\mathbf{Y}^t)]^m \left\|I(\mathbf{Y}^t) - c_1\right\|^2, \quad \text{(A.9)}$$

and

$$f_C(\mathbf{X}^t) = [u(\mathbf{X}^t)]^m f_{C_1}(\mathbf{Y}^t),\ \mathbf{X}^t, \mathbf{Y}^t \in \Omega \equiv \Re^2. \quad \text{(A.10)}$$

Therefore $F_{C_1}(\mathbf{Y}^t) = \int_{\Omega} f_{C_1}(\mathbf{Y}^t) d\mathbf{Y}^t$ and $F_C(\mathbf{X}^t) = \int_{\Omega} f_C(\mathbf{X}^t) d\mathbf{X}^t$.
Here $f_{C_1} : \Omega \to \Re$ and the domain of f_{C_1} is convex.

Now differentiating Eq. (A.9) w. r. t. u, we have

$$\frac{\partial f_{C_1}}{\partial u} = -mW_{\mathbf{X}^t\mathbf{Y}^t} [1 - u(\mathbf{Y}^t)]^{m-1} \left\|I(\mathbf{Y}^t) - c_1\right\|^2.$$

Again differentiating $\frac{\partial f_{C_1}}{\partial u}$ w. r. t. u, we have

$$\frac{\partial^2 f_{C_1}}{\partial u^2} = m(m-1)W_{\mathbf{X}^t\mathbf{Y}^t} [1 - u(\mathbf{Y}^t)]^{m-2} \left\|I(\mathbf{Y}^t) - c_1\right\|^2.$$

Now $\frac{\partial^2 f_{C_1}}{\partial u^2} \geq 0$, since $m > 1$, $W_{\mathbf{X}^t\mathbf{Y}^t} \geq 0$, $u(\mathbf{Y}^t) \in [0, 1]$ and $\left\|I(\mathbf{Y}^t) - c_1\right\|^2 \geq 0$.
Since domain of f_{C_1} is convex and $\frac{\partial^2 f_{C_1}}{\partial u^2} \geq 0$, hence f_{C_1} is convex. Therefore $\forall \mathbf{Y}_1, \mathbf{Y}_2 \in \Omega$ and $\theta \in [0, 1]$. The following relation

$$\begin{aligned}&f_{C_1}\left(\theta\mathbf{Y}_1 + (1-\theta)\mathbf{Y}_2\right)\\ &\quad \leq \theta f_{C_1}\left(\mathbf{Y}_1\right) + (1-\theta) f_{C_1}\left(\mathbf{Y}_2\right)\end{aligned} \quad \text{(A.11)}$$

holds. Integrating both the sides, we have

$$\begin{aligned}&\int_{\Omega} f_{C_1}\left(\theta\mathbf{Y}_1 + (1-\theta)\mathbf{Y}_2\right) d\mathbf{Y}^t\\ &\leq \theta \int_{\Omega} f_{C_1}\left(\mathbf{Y}_1\right) d\mathbf{Y}^t + (1-\theta) \int_{\Omega} f_{C_1}\left(\mathbf{Y}_2\right) d\mathbf{Y}^t,\ \forall \mathbf{Y}^t \in \Omega.\end{aligned} \quad \text{(A.12)}$$

But $F_{C_1} = \int_{\Omega} f_{C_1}\left(\mathbf{Y}\right) d\mathbf{Y}^t$, hence F_{C_1} is convex. Since f_{C_1} is convex and $[u(\mathbf{X}^t)]^m \geq 0$, then $f_C = [u(\mathbf{X}^t)]^m f_{C_1}$ is also convex.

Again let $\overline{F_C} = [u(\mathbf{X}^t)]^m F_{C_1}$. Since F_{C_1} is convex and $[u(\mathbf{X}^t)]^m \geq 0$, therefore $\overline{F_C}$ is also convex. Therefore $\forall \mathbf{X}_1, \mathbf{X}_2 \in \Omega$ and $\theta \in [0, 1]$. The following equation

$$\begin{aligned}&\overline{F_C}\left(\theta\mathbf{X}_1 + (1-\theta)\mathbf{X}_2\right)\\ &\quad \leq \theta\overline{F_C}\left(\mathbf{X}_1\right) + (1-\theta)\overline{F_C}\left(\mathbf{X}_2\right)\end{aligned} \quad \text{(A.13)}$$

holds. Then integrating both the sides, we have

$$\begin{aligned}&\int_{\Omega}\overline{F_C}\left(\theta\mathbf{X}_1+(1-\theta)\mathbf{X}_2\right)d\mathbf{X}^t\\&\leq\theta\int_{\Omega}\overline{F_C}\left(\mathbf{X}_1\right)d\mathbf{X}^t+(1-\theta)\int_{\Omega}\overline{F_C}\left(\mathbf{X}_2\right)d\mathbf{X}^t,\forall\mathbf{X}^t\in\Omega.\end{aligned}\tag{A.14}$$

Therefore $F_C=\int_{\Omega}\overline{F_C}\left(\mathbf{X}\right)d\mathbf{X}^t=\int_{\Omega}\left[u(\mathbf{X}^t)\right]^m F_{C_1}d\mathbf{X}^t$ is convex. In a similar way, it can be shown that

$$\begin{aligned}F_D=&\int_{\Omega}\left[1-u(\mathbf{X}^t)\right]^m\\&\left\{\int_{\Omega}W_{\mathbf{X}^t\mathbf{Y}^t}\left[u(\mathbf{Y}^t)\right]^m\left\|I(\mathbf{Y}^t)-c_2\right\|^2d\mathbf{Y}^t\right\}d\mathbf{X}^t\end{aligned}\tag{A.15}$$

is also convex. Since $0\leq\beta\leq1$, $1-\beta\geq0$, $\lambda_1,\lambda_2>0$, then F is the weighted sum of four (F_A, F_B, F_C, and F_D) convex functions. i.e.,

$$F=\lambda_1\beta F_A+\lambda_2\beta F_B+\lambda_1(1-\beta)F_C+\lambda_2(1-\beta)F_D.$$

Hence, F is convex with respect to u. Therefore, the proposed energy function is convex with respect to membership function $u(\mathbf{X}^t)$.

B :Appendix

Since an image is discrite in nature, instead of integration, summation is considered here.

Let us assume two prototypes c_1 and c_2 which approximate the image intensity $inside(C)$ and $outside(C)$ the contour C. Thus it can be written as

$$c_1=\frac{\sum_{\Omega}\left[u(X)\right]^mI(X)}{\sum_{\Omega}\left[u(X)\right]^m}\tag{B.1}$$

and

$$c_2=\frac{\sum_{\Omega}\left[1-u(X)\right]^mI(X)}{\sum_{\Omega}\left[1-u(X)\right]^m},\tag{B.2}$$

where $I(X)$ is the intensity value at pixel location X, $u(X)$ is the degree of membership of pixel X inside C, and m is the fuzzifier which determines the fuzziness present in the given image.

Therefore, total fuzzy energy for the whole image can be computed as

$$\begin{aligned}&F=\lambda_1\beta\sum_{\Omega}\left[u(X)\right]^m\left\|I(X)-c_1\right\|^2\\&+\lambda_2\beta\sum_{\Omega}\left[1-u(X)\right]^m\left\|I(X)-c_2\right\|^2\\&+\lambda_1(1-\beta)\sum_{\Omega}\left[u(X)\right]^mh_1\\&+\lambda_2(1-\beta)\sum_{\Omega}\left[1-u(X)\right]^mh_2\\&=F_A+F_B+F_C+F_D.\end{aligned}\tag{B.3}$$

where

$$\begin{aligned}F_A&=\lambda_1\beta\sum_{\Omega}\left[u(X)\right]^m\left\|I(X)-c_1\right\|^2,\\F_B&=\lambda_2\beta\sum_{\Omega}\left[1-u(X)\right]^m\left\|I(X)-c_2\right\|^2,\\F_C&=\lambda_1(1-\beta)\sum_{\Omega}\left[u(X)\right]^mh_1,\\F_D&=\lambda_2(1-\beta)\sum_{\Omega}\left[1-u(X)\right]^mh_2,\end{aligned}\tag{B.4}$$

with

$$\begin{aligned}h_1&=\sum_{\Omega}W_{XY}\left[1-u(Y)\right]^m\left\|I(Y)-c_1\right\|^2,\\h_2&=\sum_{\Omega}W_{XY}\left[u(Y)\right]^m\left\|I(Y)-c_2\right\|^2.\end{aligned}\tag{B.5}$$

Let us assume that a pixel $P\in I$ with intensity I_o and degree of membership u_o. If we change the degree of membership of pixel P to the value u_n using Eq. (18), then c_1 and c_2 will be changed to new values $\overline{c_1}$ and $\overline{c_2}$, respectively. The new values of c_1 and c_2 are calculated as

$$\begin{aligned}\overline{c_1}&=\frac{\sum_{\Omega}\left[\overline{u}(X)\right]^mI(X)}{\sum_{\Omega}\left[\overline{u}(X)\right]^m}\\&=\frac{\sum_{\Omega}\left[u(X)\right]^mI(X)+\left(u_n^m-u_o^m\right)I_o}{\sum_{\Omega}\left[u(X)\right]^m+u_n^m-u_o^m}\\&=\frac{c_1\sum_{\Omega}\left[u(X)\right]^m+\left(u_n^m-u_o^m\right)I_o}{\sum_{\Omega}\left[u(X)\right]^m+u_n^m-u_o^m}\\&=\frac{c_1a_1+\left(u_n^m-u_o^m\right)I_o}{a_1+u_n^m-u_o^m}\\&=\frac{c_1\left(a_1+u_n^m-u_o^m\right)-c_1\left(u_n^m-u_o^m\right)+\left(u_n^m-u_o^m\right)I_o}{a_1+u_n^m-u_o^m}\\&=c_1+\frac{\left(u_n^m-u_o^m\right)I_o-c_1\left(u_n^m-u_o^m\right)}{a_1+u_n^m-u_o^m}\\&=c_1+\frac{\left(u_n^m-u_o^m\right)\|I_o-c_1\|}{a_1+u_n^m-u_o^m}\\&=c_1+S_1\|I_o-c_1\|\end{aligned}\tag{B.6}$$

where $a_1=\sum_{\Omega}\left[u\left(X\right)\right]^m$ and $S_1=\frac{u_n^m-u_o^m}{\sum_{\Omega}\left[u(X)\right]^m+u_n^m-u_o^m}$ $=\frac{u_n^m-u_o^m}{a_1+u_n^m-u_o^m}$.

Similarly,

$$\begin{aligned}\overline{c_2}&=\frac{\sum_{\Omega}\left[1-\overline{u}(X)\right]^mI(X)}{\sum_{\Omega}\left[1-\overline{u}(X)\right]^m}\\&=c_2+\frac{\left[(1-u_n)^m-(1-u_o)^m\right]\|I_o-c_2\|}{a_2+(1-u_n)^m-(1-u_o)^m}=c_2+S_2\|I_o-c_2\|\end{aligned}\tag{B.7}$$

where $a_2=\sum_{\Omega}\left[1-u\left(X\right)\right]^m$ and $S_2=\frac{(1-u_n)^m-(1-u_o)^m}{a_2+(1-u_n)^m-(1-u_o)^m}$.

From Eq. (15), it is seen that if degree of membership $u(X)$ is changed, then the energy of the model will also be changed. If F denotes the old energy and $\overline{F}$ denotes the new energy due to changing of degree of membership of the point P, then

$$\overline{F}=\overline{F}_A+\overline{F}_B+\overline{F}_C+\overline{F}_D,\tag{B.8}$$

with

$$\begin{aligned}\overline{F}_A&=\lambda_1\beta\sum_{\Omega}\left[\overline{u}\left(X\right)\right]^m\left\|I(X)-\overline{c_1}\right\|^2\\&=\lambda_1\beta\left\{\sum_{\Omega}\left[u\left(X\right)\right]^m\left\|I(X)-\overline{c_1}\right\|^2+\left(u_n^m-u_o^m\right)\left\|I_o-\overline{c_1}\right\|^2\right\}\\&=F_A+\lambda_1\beta\|I_o-c_1\|^2\left[a_1+\left(u_n^m-u_o^m\right)\right]S_1\left(\frac{a_1}{a_1+\left(u_n^m-u_o^m\right)}\right)\\&=F_A+\lambda_1\beta S_1a_1\|I_o-c_1\|^2.\end{aligned}\tag{B.9}$$

Similarly,

$$\overline{F}_B=F_B+\lambda_2\beta a_2S_2\|I_o-c_2\|^2.\tag{B.10}$$

Then

$$\begin{aligned}\overline{F}_C=&\lambda_1\left(1-\beta\right)\sum_{\Omega}\left[\overline{u}\left(X\right)\right]^m\\&\left\{\sum_{\Omega}W_{XY}\left[1-u\left(Y\right)\right]^m\left\|I(Y)-\overline{c}_1\right\|^2\right\}\\=&\lambda_1\left(1-\beta\right)\sum_{\Omega}\left[u\left(X\right)\right]^m\\&\left\{\sum_{\Omega}W_{XY}\left[1-u\left(Y\right)\right]^m\left\|I(Y)-\overline{c}_1\right\|^2\right\}\\&+\lambda_1\left(1-\beta\right)\left(u_n^m-u_o^m\right)\\&\left\{\sum_{\Omega}W_{oY}\left[1-u\left(Y\right)\right]^m\left\|I(Y)-\overline{c}_1\right\|^2\right\}\\&+\lambda_1\left(1-\beta\right)\left(u_n^m-u_o^m\right)\\&\left\{\sum_{\Omega}W_{oY}\left[1-u\left(Y\right)\right]^m\left\|I_o-\overline{c}_1\right\|^2\right\}.\end{aligned}\tag{B.11}$$

Let

$$\begin{aligned}
\overline{F}_{C_1} &= \lambda_1(1-\beta)\sum_{\Omega}[u(X)]^m \\
&\quad \left\{\sum_{\Omega} W_{XY}\left[1-u(Y)\right]^m \|I(Y)-\overline{c}_1\|^2\right\}, \\
\overline{F}_{C_2} &= \lambda_1(1-\beta)\left(u_n^m-u_o^m\right) \\
&\quad \left\{\sum_{\Omega} W_{oY}\left[1-u(Y)\right]^m \|I(Y)-\overline{c}_1\|^2\right\}, \\
\overline{F}_{C_3} &= \lambda_1(1-\beta)\left(u_n^m-u_o^m\right) \\
&\quad \left\{\sum_{\Omega} W_{oY}\left[1-u(Y)\right]^m \|I_o-\overline{c}_1\|^2\right\}.
\end{aligned} \tag{B.12}$$

Now,

$$\begin{aligned}
\overline{F}_{C_1} &= \lambda_1(1-\beta)\sum_{\Omega}[u(X)]^m \\
&\quad \left\{\sum_{\Omega} W_{XY}\left[1-u(Y)\right]^m \|I(Y)-\overline{c}_1\|^2\right\} \\
&= F_C + \lambda_1(1-\beta)\sum_{\Omega}[u(X)]^m \\
&\quad \left\{\sum_{\Omega} W_{XY}\left[1-u(Y)\right]^m S_1^2\|I_o-c_1\|^2\right\} \\
&-2\lambda_1(1-\beta)\sum_{\Omega}[u(X)]^m \\
&\quad \left\{\sum_{\Omega} W_{XY}\left[1-u(Y)\right]^m \|I(Y)-c_1\|S_1\|I_o-c_1\|\right\}.
\end{aligned} \tag{B.13}$$

$$\begin{aligned}
\overline{F}_{C_2} &= \lambda_1(1-\beta)\left(u_n^m-u_o^m\right) \\
&\quad \left\{\sum_{\Omega} W_{oY}\left[1-u(Y)\right]^m \|I(Y)-\overline{c}_1\|^2\right\} \\
&= \lambda_1(1-\beta)\left(u_n^m-u_o^m\right) \\
&\quad \left\{\sum_{\Omega} W_{oY}\left[1-u(Y)\right]^m \|I(Y)-c_1-S_1(I_o-c_1)\|^2\right\}.
\end{aligned} \tag{B.14}$$

$$\begin{aligned}
\overline{F}_{C_3} &= \lambda_1(1-\beta)\left(u_n^m-u_o^m\right) \\
&\quad \left\{\sum_{\Omega} W_{oY}\left[1-u(Y)\right]^m \|I_o-\overline{c}_1\|^2\right\} \\
&= \lambda_1(1-\beta)\left(u_n^m-u_o^m\right) \\
&\quad \left\{\sum_{\Omega} W_{oY}\left[1-u(Y)\right]^m \|I_o-c_1\|^2\left[1-S_1\right]^2\right\}.
\end{aligned} \tag{B.15}$$

Therefore, we have $\overline{F}_C = \overline{F}_{C_1} + \overline{F}_{C_2} + \overline{F}_{C_3}$.

$$\begin{aligned}
\overline{F}_C &= F_C + \lambda_1(1-\beta)\sum_{\Omega}[u(X)]^m \\
&\quad \left\{\sum_{\Omega} W_{XY}\left[1-u(Y)\right]^m S_1^2\|I_o-c_1\|^2\right\} \\
&-2\lambda_1(1-\beta)\sum_{\Omega}[u(X)]^m \\
&\quad \left\{\sum_{\Omega} W_{XY}\left[1-u(Y)\right]^m \|I(Y)-c_1\|S_1\|I_o-c_1\|\right\} \\
&+\lambda_1(1-\beta)\left(u_n^m-u_o^m\right) \\
&\quad \left\{\sum_{\Omega} W_{oY}\left[1-u(Y)\right]^m \|I(Y)-c_1-S_1(I_o-c_1)\|^2\right\} \\
&+\lambda_1(1-\beta)\left(u_n^m-u_o^m\right) \\
&\quad \left\{\sum_{\Omega} W_{oY}\left[1-u(Y)\right]^m \|I_o-c_1\|^2\left[1-S_1\right]^2\right\}.
\end{aligned} \tag{B.16}$$

Similarly, we have

$$\begin{aligned}
\overline{F}_D &= F_D + \lambda_2(1-\beta)\sum_{\Omega}[1-u(X)]^m \\
&\quad \left\{\sum_{\Omega} W_{XY}\left[u(Y)\right]^m S_2^2\|I_o-c_2\|^2\right\} \\
&-2\lambda_2(1-\beta)\sum_{\Omega}[1-u(X)]^m \\
&\quad \left\{\sum_{\Omega} W_{XY}\left[u(Y)\right]^m \|I(Y)-c_2\|S_2\|I_o-c_2\|\right\} \\
&+\lambda_2(1-\beta)\left[(1-u_n)^m-(1-u_o)^m\right] \\
&\quad \left\{\sum_{\Omega} W_{oY}\left[u(Y)\right]^m \|I(Y)-c_2-S_2(I_o-c_2)\|^2\right\} \\
&+\lambda_2(1-\beta)\left[(1-u_n)^m-(1-u_o)^m\right] \\
&\quad \left\{\sum_{\Omega} W_{oY}\left[u(Y)\right]^m \|I_o-c_2\|^2\left[1-S_2\right]^2\right\}.
\end{aligned} \tag{B.17}$$

Therefore, we have

$$\begin{aligned}
\overline{F} &= \overline{F}_A + \overline{F}_B + \overline{F}_C + \overline{F}_D \\
&= F + \lambda_1\beta S_1 a_1\|I_o-c_1\|^2 + \lambda_2\beta S_2 a_2\|I_o-c_2\|^2 \\
&-2\lambda_1(1-\beta)S_1\|I_o-c_1\|b_1 + \lambda_1(1-\beta)g_1\left[\|c_1+S_1(I_o-c_1)\|^2-\|c_1\|^2\right] \\
&+\lambda_1(1-\beta)\left(u_n^m-u_o^m\right) \\
&\quad \left\{\sum_{\Omega} W_{oY}\left[1-u(Y)\right]^m \|I(Y)-c_1-S_1(I_o-c_1)\|^2\right\} \\
&+\lambda_1(1-\beta)\left(u_n^m-u_o^m\right) \\
&\quad \left\{\sum_{\Omega} W_{oY}\left[1-u(Y)\right]^m \|I_o-c_1\|^2\left[1-S_1\right]^2\right\} \\
&-2\lambda_2(1-\beta)S_2\|I_o-c_2\|b_2 \\
&+\lambda_2(1-\beta)g_2\left[\|c_2+S_2(I_o-c_2)\|^2-\|c_2\|^2\right] \\
&+\lambda_2(1-\beta)\left[(1-u_n)^m-(1-u_o)^m\right] \\
&\quad \left\{\sum_{\Omega} W_{oY}\left[u(Y)\right]^m \|I(Y)-c_2-S_2(I_o-c_2)\|^2\right\} \\
&+\lambda_2(1-\beta)\left[(1-u_n)^m-(1-u_o)^m\right] \\
&\quad \left\{\sum_{\Omega} W_{oY}\left[u(Y)\right]^m \|I_o-c_2\|^2\left[1-S_2\right]^2\right\}.
\end{aligned} \tag{B.18}$$

Thus the energy difference ΔF between old energy (F) and new energy ($\overline{F}$) due to change of degree of membership value can be obtained as

$$\begin{aligned}
\Delta F &= \overline{F} - F \\
&= \lambda_1\beta S_1 a_1\|I_o-c_1\|^2 \\
&+\lambda_2\beta S_2 a_2\|I_o-c_2\|^2 \\
&-2\lambda_1(1-\beta)S_1\|I_o-c_1\|b_1 \\
&+\lambda_1(1-\beta)g_1\left[\|c_1+S_1(I_o-c_1)\|^2-\|c_1\|^2\right] \\
&+\lambda_1(1-\beta)\left(u_n^m-u_o^m\right) \\
&\quad \left\{\sum_{\Omega} W_{oY}\left[1-u(Y)\right]^m \|I(Y)-c_1-S_1(I_o-c_1)\|^2\right\} \\
&+\lambda_1(1-\beta)\left(u_n^m-u_o^m\right) \\
&\quad \left\{\sum_{\Omega} W_{oY}\left[1-u(Y)\right]^m \|I_o-c_1\|^2\left[1-S_1\right]^2\right\} \\
&-2\lambda_2(1-\beta)S_2\|I_o-c_2\|b_2 \\
&+\lambda_2(1-\beta)g_2\left[\|c_2+S_2(I_o-c_2)\|^2-\|c_2\|^2\right] \\
&+\lambda_2(1-\beta)\left[(1-u_n)^m-(1-u_o)^m\right] \\
&\quad \left\{\sum_{\Omega} W_{oY}\left[u(Y)\right]^m \|I(Y)-c_2-S_2(I_o-c_2)\|^2\right\} \\
&+\lambda_2(1-\beta)\left[(1-u_n)^m-(1-u_o)^m\right] \\
&\quad \left\{\sum_{\Omega} W_{oY}\left[u(Y)\right]^m \|I_o-c_2\|^2\left[1-S_2\right]^2\right\},
\end{aligned} \tag{B.19}$$

where

$$\begin{aligned}
a_1 &= \sum_{\Omega}[u(X)]^m \\
a_2 &= \sum_{\Omega}[1-u(X)]^m \\
S_1 &= \frac{u_n^m-u_o^m}{\sum_{\Omega}[u(X)]^m+u_n^m-u_o^m} \\
S_2 &= \frac{(1-u_n)^m-(1-u_o)^m}{\sum_{\Omega}[1-u(X)]^m+(1-u_n)^m-(1-u_o)^m} \\
b_1 &= \sum_{\Omega}[u(X)]^m\left\{\sum_{\Omega} W_{XY}\left[1-u(Y)\right]^m I(Y)\right\} \\
b_2 &= \sum_{\Omega}[1-u(X)]^m\left\{\sum_{\Omega} W_{XY}\left[u(Y)\right]^m I(Y)\right\} \\
g_1 &= \sum_{\Omega}[u(X)]^m\left\{\sum_{\Omega} W_{XY}\left[1-u(Y)\right]^m\right\} \\
g_2 &= \sum_{\Omega}[1-u(X)]^m\left\{\sum_{\Omega} W_{XY}\left[u(Y)\right]^m\right\}.
\end{aligned}$$